Elsevier Editorial System(tm) for Journal of Hydrology
Manuscript Draft

Manuscript Number:

Title: MODELING FLOOD DYNAMICS IN A TEMPORARY RIVER BASIN DRAINING TO AN EUTROPHIC RESERVOIR IN SOUTHEAST PORTUGAL (ENXOÉ)

Article Type: Research Paper

Keywords: Keywords: Enxoé, eutrophic reservoir, floods, nutrients, watershed modeling, MOHID Land model

Corresponding Author: Mr. David Brito,

Corresponding Author's Institution: Maretec - Instituto Superior Técnico - Technical University of Lisbon, Av. Rovisco Pais, 1049-001 Lisboa, Portugal

First Author: David Brito

Order of Authors: David Brito; Ramiro Neves, Ph.D; Maria A Branco; Maria C Gonçalves, Ph.D

Suggested Reviewers: Matthias Obermann Ph.D
Dorsch Consult Wasser und Umwelt GmbH
mail@matthiasobermann.de
Knowledge on flood dynamics and MOHID land model important aspects of the paper

David Cooper Ph.D
Hydrochemical Modeller, Centre for Ecology & Hydrology, Center for Ecology & Hidrology
cooper@ceh.ac.uk
knowledge on floods dynamics and modelling

Jochen Froebrich Ph.D
DLO Onderzoeker, Alterra Wageningen UR
Jochen.Froebrich@WUR.nl
knowledge on watershed modelling

Francesc Gallart Ph.D
Surface Hydrology and Erosion Group, Consejo Superior de Investigaciones Científicas
francesc.gallart@idaea.csic.es
knowledge on surface water hidrology and modelling

Ehab Meselhe
Assistant editor in similar themed articles

Attillio Castellarin
Assistant editor in similar themed articles

Emmanuel Anagnostou
Assistant editor in similar themed articles

Baxter Vieux
Assistant editor in similar themed articles

MODELING FLOOD DYNAMICS IN A TEMPORARY RIVER BASIN DRAINING TO AN EUTROPHIC RESERVOIR IN SOUTHEAST PORTUGAL (ENXOÉ)

David Brito[1]; Ramiro Neves[1]; Maria A. Branco[2]; Maria C. Gonçalves[2],

[1]Maretec, Instituto Superior Técnico, Technical University of Lisbon, Av. Rovisco Pais, 1049-001 Lisboa

[2] Instituto Nacional de Recursos Biológicos, Quinta do Marquês, Av. República, 2784-505 Oeiras, Portugal.

First author and corresponding author: David Brito, e-mail: david.maretec@ist.utl.pt, tel: 00351 218419425

Abstract

Enxoé reservoir was built in 1998 and since 2000 occurred frequent high chlorophyll-a concentrations (reaching geometric means 6 times the national limit for eutrophication of 10 $\mu g.L^{-1}$), representing the reservoir with the higher eutrophic state in Portugal. Enxoé is a temporary river with tendency to flushy regime and the flood dynamics, that may impact reservoir state, was characterized using the following approach: i) collect data in the, until then, ungauged watershed (2010-2011); ii) implement MOHID Land model and validate the hydrology against existing data, and iii) with the model validated, quantify flood role on annual loads and depict flood dynamics (Normalized Cumulative Discharge and Load). MOHID Land model results obtained satisfactory to good agreement with field data (monthly flows with R^2 of 0.88 and Nash-Sutcliffe efficiencies of 0.88; hourly flood levels with R^2 > 0.25 and Nash-Sutcliffe efficiencies > 0.60).

It was observed that soil loss of permeability in Enxoé is an important factor to accurately predict first floods or first peaks of consecutive floods and cumulative load results with orders similar to urbanized watersheds reinforced this fact. First floods in the year had a lower weight in terms of annual volume and annual nutrient load to the reservoir (less than 3% and 7% respectively) that floods in winter (between 10%-20% each). However, first floods in the year transported particulated concentrations that were 5 to 50 times the low waters value (and most of the transport occurred in the first minutes of flood, before flow peak, from deposited material in river bed and in neighbor land areas), while in winter, concentration remained almost constant during flood. Further work should link watershed models to a reservoir model in order to depict the flood impact in the reservoir and test management strategies to reduce reservoir trophic state.

Keywords: Enxoé, eutrophic reservoir, floods, nutrients, watershed modeling, MOHID Land model

1 Introduction

Enxoé reservoir was built in 1998 and since 2000 it has had frequent chlorophyll-a concentrations higher than 50 $\mu g.L^{-1}$. the geometric average of surface concentration from 1998-2009 from April to September is around 60 $\mu g.L^{-1}$ where the national limit for eutrophication is 10 $\mu g.L^{-1}$) and toxic cyanobacteria occurred (INAG, 2004 and Valério et. al. 2005). This situation provides a problem for water managements in two fronts: i) the eutrophication of the reservoir in the scope of Water Framework Directive calls for management plans, and ii) the high concentration of algae and specifically the presence of toxic algae is a major issue in a reservoir that is used for water production.

Cyanobacteria algae dominance is usually described by two main processes: i) some species are able to consume N^2 dissolved in water (Paerl et al. 2001, Havens et al. 2003, Rolff et al. 2007), whereas ii) some species are able to maintain growth even under conditions of low light availability (Havens et al. 2003). The nitrogen fixation characteristic of some types of cyanobacteria allows them to be independent of the availability of inorganic forms of nitrogen (e.g., ammonia, nitrate). Furthermore, under conditions of nitrogen limitation, cyanobacteria have the potential to generate blooms if phosphorus is available (Havens, 2003).

Such a cyanobacterial response to phosphorus availability may have occurred in Enxoé reservoir after 2002 when these species started to be dominant (INAG, 2004, Coelho et al. 2008). 2000/2001 was a wet hydrologic year, and the winter floods transported adsorbed material to the reservoir. The first blooms consumed the available inorganic material while organic matter deposited. The accumulation of organic matter at the bottom of the reservoir and the corresponding increase in mineralization may have depleted the oxygen near the bottom (where mineralization is more intense); thus, under anoxic conditions, phosphorus may have been released from the absorbed phase to the water column (Lake et al. 2007, Jiang et al. 2006) and fueled blooms. These processes were noted in previous work performed at Enxoé as the probable drivers for algal blooms in Enxoé and also for cyanobacterial dominance (Coelho et al. 2008). The eutrophic status in the reservoir and the previous work done called for the characterization of the watershed dynamics and nutrient loads exported to the reservoir. Enxoé reservoir is fed by a 60 km^2 watershed with annual precipitation around 500 mm distributed from October to April (usually occurring intense and concentrated precipitation events that create flood rise and fall in couple of hours) and dry season from May to September (where flow is really low or absent – temporary river).

Since Enxoé is a small-sized watershed with fast response to precipitation events also flood dynamics may have a role on material transported to the reservoir. The overall objective of the work involved in Enxoé is to simulate watershed and reservoir dynamics to represent the actual situation and test management scenarios in both watershed and reservoir to reduce reservoir trophic state. In that scope the intended approach is to characterize long-term dynamics and flood dynamics in the watershed and then feed the reservoir model with the watershed input. The long term dynamics will be evaluated with SWAT model (spatially lumped, daily time step) and this article describes the flood analysis with MOHID Land model (spatially distributed, continuous, variable time step).

Floods

Several authors have been describing the relation between watershed characteristics and flood generation being a complex relation between rain amount, topography, soil properties and soil antecedent conditions (James and Roulet, 2009, Li et al. 2012).

The main component of floods and specifically of fast floods (or flush floods) in arid or semi-arid region (without macropore or karstic flow) is runoff water or subsurface water that arrives faster to the river than groundwater flow. In Enxoé watershed flood peaks occur within 1 to 5 hours after flood start and as a direct response of rain events.

The process of runoff generation in flush floods may have origin in water that is unable to infiltrate (because of soil impermeabilization or storm water drainage in urban areas) or if infiltration in soil occurs, the predominance of infiltration excess, subsurface stormflow or saturation excess will depend on rain intensity, soil properties (e.g. conductivity, water content, etc.) and slope (Niehoff et al. 2002). Temporary streams in arid and semi-arid areas have a dry season for several months (Enxoé usually from June to October with no flow), increasing not only organic matter accumulation in land (animal and leaf fall/residue from crop) and in river bed (Obermann et al. 2009) but also mineral form concentrations (mineralization in soil and in river pools). First floods importance on load transport is dependent on flow generated and concentration transported. First floods occur with soil in dry conditions that has capacity for infiltration and so volume transported in surface runoff and river usually is lower than same rain amount during rainy season (when soil is saturated or close). In the other end, the particulated properties concentrations in first floods are usually higher because of the referred accumulation during dry season making not linear to evaluate the flood weight in annual load and being dependent on each site.

Load or concentration with flow?

Usually watershed inputs and reduction scenarios are based on loads (mass per unit time) but also may be referred as concentration (Sansalone and Cristina, 2004). Aquatic systems biology in rivers, reservoirs or lakes respond to concentration. However, load evaluation may give insights on the extent of the concentration pattern in downstream water bodies and it is important when it changes receiving water bodies concentration. If concentration does not change (tributaries and water bodies with same concentration), higher loads represent only higher water retention time. For particulated material however the increase in load is more linked to increase in concentration as it produces accumulation (deposition when transport velocity is reduced promoting particulate property retention time higher than water retention time).

In this article it is presented the flood loads in Enxoé but also the concentration and volume of each flood since it may be important for downstream reservoir ecological behavior.

Permeability loss/soil sealing

One aspect that also may influence flood formation is soil sealing as reduces infiltration and promotes runoff formation. Soil surface sealing may result from i) compaction (e.g. livestock, urban impermeabilization); ii) fire, iii) biological activity or iv) rain (Assouline, 2004). Rain may also have a compact effect, destroy soil aggregates and the released material may fill soil pores – locally generated or transported by runoff (Assouline and Ben-Hur, 2006). These processes were studied in arid and semi-arid regions (NE Spain) in Ramos et al. (2000) or Singer and Le Bissonnais, (1998), where the soil susceptibility to sealing was highly correlated with the high silt and low organic matter content of the soils. Moreover, micromorphological observations in Panini et al. (1997) revealed that pores in tilled soils lost their continuity in the vertical direction because of a preferential pore orientation parallel to the soil surface and Li et al. (2009) showed that wheeling energy had higher impact on soil surface degradation than rainfall energy. In Enxoé, silty soils occur and approximately 60% of the total area (occupied by olive trees and annual crops) has tillage and/or wheeling and in montado area (30% of the total area) extensive cattle production exists. The observation in Enxoé of river flood events even after dry season as a direct response to first rain events, suggest that soil sealing and/or compaction/impermeabilization may be an important process on first flood formation.

Flood simulation

Floods have an important impact on flooded areas and in the downstream water bodies. Monitoring data is usually scarce, specially in cases where floods rise within minutes to hours and collection frequency need to be high (need for automatic schemes that are costly). As so, in order to fill data gaps and to be able to predict their occurrence, models have been developed specially suited for floods.

The first feature needed to simulate a flood is that he model has to have a time step that can represent the flood rise and fall; in flush floods that may represent hourly or sub-hourly time steps (Boughton and Droop, 2003). The second feature, since in flush floods most of the water in the river arrives from surface water or storm drainage systems (in urban areas) than the model should be able to simulate impermeabilization (e.g. roofs, roads, and other structures), runoff generation and routing and storm drainage systems (Hsu et al. 2000).

Watershed models traditionally put their efforts on describing long-term dynamics and to enhance computation time, time steps are of the order of one day or one hour as SWAT model (Neitsch et al., 1998) and HSPF (Bicknell et al., 1993), respectively, making them not suited for fast flood analysis. However, other models exist that have lower time steps suited for floods as KINEROS (Woolhiser et al., 1990), MIKE 11 from Dutch Hydraulic Institute (Havnø et al. 1995) or HEC-RAS from Army Corp of Engineers (Brunner, 2010). The first is spatially lumped and uses kinematic wave that does not allow back water effects (flow is driven by terrain slope), and the latter resolve both complete St. Venant equations (that accomplish back water effects and inertia) using finite differences. The latter models are limited to the description of river hydraulics and both need to be given boundary conditions for surface and groundwater discharges; MIKE 11 however may be coupled to Systeme Hydrologique Europeen (SHE) model (Abbott et al. 1986a and Abbott et al. 1986b) as in Thompson et al. (2004).

MOHID Land model is developed by Instituto Superior Técnico in Technical University of Lisbon and is a distributed (grid-based), continuous, variable time step watershed model that includes processes in atmosphere (model forcing), interception and evaporation in leafs, infiltration and evapotranspiration in soil, and routing of water trough surface runoff, porous media or river network using a finite volume approach based on mass and momentum balance equations. In the river the complete St. Venant equations are solved in 1D (Trancoso, 2009) and for runoff the same equations are derived for 2D and Richard’s equation is used for 3D porous media in a continuous medium between saturated and unsaturated zones. MOHID modeling system integrates all the mediums (surface water, porous media, and river) in a continuous way in order to avoid the need for imposing boundary conditions and the finite volume approach guarantees mass conservation. MOHID Land solves the main processes that control the water cycle in a watershed in a modular way what allows the easily inclusion of new processes or new formulation of the same process. MOHID Land also solves property transport and transformation but these processes are out of the scope of the present article.

The specific objectives for the MOHID Land model application in Enxoé were: i) implement and validate MOHID Land model in long-term flow and flood events and ii) quantify the role of floods (including first) in annual dynamics. Enxoé watershed was ungauged so long-term flow validation was performed with reservoir estimated inflow (from measured precipitation, evaporation and discharges); flood validation was performed with water level automatically measured in floods. Loads were computed with the validated model flow and measured concentration.

The long-term assessment of input loads to the reservoir and water and nutrient balance was performed in Brito et al. (submitted) implementing SWAT model to the watershed in a 30 year period being validated for flow, suspended solids and nutrient. It was found that in Enxoé in average annually around 80-85% of precipitation is evapotranspired and nutrient exports for nitrogen are around 2.5-2.8 $kg.ha^{-1}.year^{-1}$ and for phosphorus around 0.3 $kg.ha^{-1}.year^{-1}$, consistent with extensive agriculture, gentle slopes and low human occupation.

In the next chapters it will be presented the study area and modeling approach followed by results (validation and flood analysis).

2 Material and Methods

2.1 Study area

Enxoé is a 60 km^2 watershed located in southeast Portugal in the left margin of the Guadiana River – Figure 1. The main river is Ribeira do Enxoé that has a length of around 10 km from headwaters up to the reservoir. Enxoé reservoir wall approximate coordinates are 37º 59' 38.121'' N, 7º 27' 54.776'' W having the reservoir a total volume of 10.4 hm^3 a surface area around 2 km^2 and an average depth of 5m.

Enxoé has annual average precipitation of 500 mm and is a temporary river with flow in the winter as a response to rain events and decreasing flow in spring after rain ceases and no flow and pool formation during summer or in low flow conditions. Slopes are low with average river slope of about 2% and watershed average slope of 5-6%. The existence of low slopes and some flatter areas promote water pooling and the occurrence of disconnected flows.

The main land uses in Enxoé are olive trees, oak-pasture mixed system (”montado”) and annual crops (each with around 30% of total area) - Figure 4 and Table 3. The annual crops are wheat, oats and sunflower.

The soil in Enxoé has its origin mainly in granite and limestone (each with around 30% of total area) and schist with around 10%.

Approximately 1000 inhabitants live in Enxoé watershed (mostly in the only village Vale de Vargo) and the Waste Water Treatment Plant (WWTP) that serves the population, since 2006 discharges outside the watershed as a protective measure to the Enxoé reservoir.

Extensive production of cows and sheep are the most important animal farming activity. According to 1999 agricultural census (INE – Instituto Nacional de Estatística) there were about 600 cows (10 per km^2) and 4200 sheep (70 per km^2) in the catchment.

Enxoé watershed was ungauged so in order to quantify nutrient export and validate the model, field activities have been conducted in 2010 and 2011 with river sampling (automatic sampling during floods and manual sampling otherwise) in the two main tributaries – Figure 2 .

2.2 MOHID Land model description

MOHID Land is an integrated model with four compartments or mediums (atmosphere, porous media, soil surface and river network) and water moves through the mediums based on mass and momentum balances. The atmosphere is not explicitly simulated but provides data necessary for imposing surface boundary conditions to the model (precipitation, solar radiation, wind, etc.) that may be space and time variant. Surface land is described by a 2D horizontal grid that can have variable spatial step. The porous media is a 3D domain with the same horizontal grid as surface, adding a vertical grid, also allowing variable layer thickness. The river network is a 1D domain defined from DTM by reaches linking surface cell centers (Figure 1).

Mohid Land model uses a finite volume approach (control volume) for computing state variables and fluxes. Each grid cell is a control volume, being the state variables computed in their centers and the fluxes (and related variables) on the faces. Mohid Land uses a variable time step approach decreasing it for high fluxes (e.g. high rain intensities and floods) and increasing it during dry season, making it suitable for flood simulation and yearly basis in a continuous way.

MOHID Land processes are based in mass conservation equation, momentum equation (derived from Newton's second law) and continuity equation (derived from mass conservation when water is the property transported).

Mass conservation equation applied to a control volume in its simple form states that the accumulation rate of a property inside the control volume is equal to the property transport trough the faces (advection and diffusion) plus the sources and sinks of property inside the volume (property transformation) as seen in (1).

$$\{AccumulationRate\}_{cv} = \{Inputs - Outputs\}_{faces}^{advection} + \{InPuts - Outputs\}_{faces}^{diffusion} + \{Sources - Sinks\}_{cv}$$ (1)

And in the integral form is obtained equation (2) where β is the property transported (kg.m^3), v is the face velocity (m.s^{-1}) and γ is face diffusivity (m^2.s^{-1}):

$$\frac{\partial}{\partial t}\iiint_{Vol} \beta \, dVol = -\iint_{A} \left(\beta \vec{v}.\vec{n}\right) dA + \iint_{A} \left(\gamma \vec{\nabla}\beta.\vec{n}\right) dA + \{Sources - Sinks\} \quad (2)$$

In the differential form (when volume tends to zero) the equation is presented in (3) where subscript $_i$ indicates flow directions, *Area* is cross section area (m^2) and *Vol* is water volume (m^3):

$$\frac{\partial \beta}{\partial t} = -\frac{\partial\left(\beta \vec{v}_i\right)}{\partial x_i} + \frac{\partial}{\partial x_i}\left(\gamma \frac{\partial \beta}{\partial x_i}\right) + \{Sources - Sinks\} \quad (3)$$

In MOHID Land equations are solved in the integral form (discretized to control volumes) but the differential form is presented for illustration. The latter equations allow solving property fields values (e.g. concentration) in any volume given velocity and diffusivity. Diffusivity is proportional to the product between molecule velocity component not described by the definition of velocity and the length of the path associated to that component and in surface water is defined by the user for each property, and in porous media a dynamic approach using tortuosity and dispersion to account for pore paths is used (Jury et al. 1991).

Velocity field is obtained from momentum equation derived from Newton's second law:

$$\{Acceleration\} = \{\mathrm{Result\ of\ Forces}\} \quad (4)$$

And in differential form where subscript $_I$ and $_j$ are flow directions and ρ is water density (kg.m^{-3}):

$$\rho Vol\left(\frac{\partial v_i}{\partial t} + v_j \frac{\partial v_i}{\partial x_j}\right) = \sum \{Forces\} \quad (5)$$

In surface water (runoff and river flow) the sum of forces are pressure represented by surface level gradient, $\frac{\partial H}{\partial x_i}$ (-), gravity by its acceleration, g (m.s^{-2}) and bottom friction, Sf_i (-):

$$\sum\{Forces\} = -\rho Vol\, g\left(\frac{\partial H}{\partial x_i} + Sf_i\right) \quad (6)$$

Sf_i is computed with Manning Strickler equation where *n* is manning rugosity ($s.m^{-1/3}$) and R_h is hydraulic radius (m):

$$\left(S_f\right)_i = \frac{n^2 |Q| Q_i}{A_v{}^2 R_h^{\frac{4}{3}}} \quad (7)$$

Combining eq. 5, 6 and 7 it is obtained St. Venant Equation (8) where *Q* is water flow ($m^3 .s^{-1}$), A_v is the cross flow area (m^2), *g* is gravity acceleration ($m.s^{-2}$), *h* is water depth (m), $\left(S_0\right)_i = -\partial z / \partial x_i$ (-) is the bottom slope, S_f is the bottom friction slope (i.e. the slope that balances the friction force) and subscript $_I$ *and* $_j$ denotes the flow directions (one in river and two in runoff).

$$\frac{\partial Q_i}{\partial t} + v_j \frac{\partial Q_i}{\partial x_j} + gA_v\left(\frac{\partial h}{\partial x_i} - \left(S_0\right)_i + \left(S_f\right)_i\right) = 0 \quad (8)$$

The water level in each cell (runoff or river) is obtained from continuity equation:

$$\frac{\partial A_v}{\partial t} + \frac{\partial Q_i}{\partial x_i} = 0 \quad (9)$$

MOHID Land river equations and processes are described in detail in Trancoso et al, 2009 and runoff is a 2D implementation of the same general equation being both derived from Newton's second law and continuity equation.

Porous Media in MOHID Land is a 3D domain including saturated and non saturated cells in a continuous way (differing in water content). In the porous media, from Newton's second law, the sum of the forces is the pressure represented by hydraulic head gradient, $\frac{\partial H}{\partial x_i}$ (-), gravity acceleration and resistance, $\frac{v_i}{K}$ (-) where K is conductivity ($m.s^{-1}$) and H is hydraulic head (m):

$$\sum\{Forces\} = -\rho Vol\, g\left(\frac{\partial H}{\partial x_i} + \frac{v_i}{K}\right) \quad (10)$$

Combining equation 5 and 10, assuming that soil inertia is negligible (velocities are low and resistance balances pressure) and using the conductivity concept we get the Richards equation for porous media:

$$\frac{\partial \theta}{\partial t} = \frac{\partial}{\partial x_i}\left(K(\theta)\left(\frac{\partial h}{\partial x_i} + \frac{\partial z}{\partial x_i}\right)\right) \quad (11)$$

Where, θ is water content (-), h is suction head (m) and z is altitude relative to Mean Sea Level (m) and $_i$ are the flow directions.

Vegetation model used in MOHID Land was adapted from the SWAT model (Neitsch et al. 2005) computing heat units for driving plant activity and using SWAT crop database for plant potential growth curves. Actual growth is then computed accounting for limitations due to environmental constraints (water availability, temperature, nutrients, etc.). Reference evapotranspiration (ET_r) may be given by the user or computed using the FAO Penman Montheith method. Crop evapotranspiration (ET_c) is obtained from k_c (crop coefficient, adimensional):

$$ET_c = K_c * ET_r \quad (12)$$

The separation between potential transpiration (PotTransp) and potential evaporation (PotEvap) from crop evapotranspiration is done with Leaf Area Index (LAI, $m^2.m^{-2}$) from Ritchie, 1972:

$$PotTransp = ET_c * (1 - Exp(-0.463 * LAI)) \quad (13)$$

$$PotEvap = ET_c - PotTransp \quad (14)$$

Actual transpiration is computed from potential transpiration as a function of root distribution and soil water availability (from Feddes et al. 2001) and actual evaporation may be limited from potential evaporation by head threshold or by conductivity since evaporation lowers with drying (ASCE, 1996).

Water exchanges between the river and the porous media are computed using the head gradient and between the river and land surface using the surface gradient. For exchanges with porous media the Richards equation is used, considering the head in the river as the free surface level. These algorithms

permit the explicit simulation of river floods and generate variable river discharge, as a function of the water content and flow along the whole catchment.
MOHID Land model shares the knowledge of fluid mechanics, hydrology and water quality of MOHID Water model (developed from the 80's with several publications) and is an open source model (www.mohid.com and mohid.codeplex.com) in which validation work published is the work of Trancoso et al. (2009) in a 300 km^2 urban and agricultural watershed and Barão et al. (2010) in a plot scale irrigation project. Being a open source model other teams (beside the developing team in Instituto Superior Técnico) have successfully applied it to water quality applications in river La Véne, France (Boutron et al. 2010) and in lake Kinneret, Israel (Gaßmann et al. 2009), in erosion patterns in river Save, France (Bailly et al. 2010). Also other projects are underway where MOHID land application will go from irrigation service to farmers (www.agro-evapo.eu/), water management in 4 world wide locations (mywater-fp7.eu/) up to provide flood forecast for coastal water quality models (www.lenvis.eu).

2.2.1 Modeling approach

As described above, the objective is to implement MOHID Land model to Enxoé watershed and: i) validate flow over long-term and flood events comparing against data; ii) with the model validated characterize 2010-2011 floods dynamics and weight on annual loads to the reservoir.
In order to implement the model, validate the model and produce useful information, data is needed and needs to be integrated. As so in next chapters it is presented the data used to implement the model, data used to validate the model and the calibrations done.

2.2.2 Data for model implementation

In Table 2 is described the data used to implement MOHID Land model to Enxoé (digital terrain model, land use, soil texture, precipitation stations, weather stations, etc.).

Land use map with classification is presented in Figure 4 and Table 3 where, as stated previously, olive trees (orchard), “montado” (oak + forest) and annual crops represent each around 30% of total area. The land use map was obtained from Corine 2000 and aerial pictures and local observation show that actual land use is still consistent with Corine map.

In annual crops the information about agricultural practices (planting and harvesting calendar) were obtained from questionnaires given to farmers. The agricultural practices in Enxoé consist of rotation between wheat and oats in land use “annual crops rotation 2” in Figure 1 and rotation between sunflower, wheat and oats in “annual crops rotation 1” (refer to Table 4 for agricultural practices definitions for each crop).

2.2.3 Data for model validation

Enxoé was an ungauged watershed in the river, thus, to define the state of the river and validate the model, data collection was performed during 2010-2011 in the two main tributaries to the Enxoé reservoir (Enxoé river and the river that passes trough the only village, entering Enxoé before the beginning of the reservoir (Figure 1). Flood data was obtained with an automatic sampler (AWS 2002) and a coupled multiparametric YSI 6000 probe (measuring level, turbidity, temperature, conductivity and oxygen). Automatic sampling was performed when measured level raised or lowered more than 10 cm. The river manual data in low water conditions was collected in a weekly basis during winter and spring and when available water existed during summer (temporary river). The parameters evaluated in laboratory were salinity, pH, nutrients, suspended solids, etc.

In terms of flow validation, monthly data from Enxoé reservoir discharges and consumption, precipitation and evaporation were used to estimate reservoir inflow (2006-2009). Level measures obtained during floods by probe in 2010-2011 were also used to validate MOHID Land ability do describe these short-term processes.

In Table 5 is described the data used for model flow validation.

2.2.4 Model Evaluation

Both qualitative and quantitative measures were used to compare the observed data and the predicted values. Graphical analyses such as time-series plots were used to identify the general trends, potential sources of error, and differences between measured and predicted values.

MOHID Land model performance was evaluated using R^2, coefficient of determination that evaluates the correlation between two series, RMSE, root mean squared error that evaluates the deviation and Nash–Sutcliffe Efficiency (NSE) which is goodness-of-fit criterion for the predicated and observed values (Nash and Sutcliffe, 1970). NSE Values between 0.0 and 1.0 are generally viewed as acceptable levels of performance, whereas values <0.0 indicates that the mean observed value is a better predictor than the simulated value, which indicates unacceptable performance (Moriasi et al., 2007).

2.2.5 Normalized Cumulative Loads

One common method to identify phases of nutrient fluxes is trough diagrams of normalized cumulative loads over normalized cumulative flow. The normalized cumulative flow (NCF) and the normalized cumulative load (NCL) of a parameter β can be calculated from:

$$NCF = \frac{\int_{t0}^{t} Q(t)dt}{\int_{t0}^{tf} Q(t)dt}$$

$$NCL = \frac{\int_{t0}^{t} \beta(t) \cdot Q(t)dt}{\int_{t0}^{tf} \beta(t) \cdot Q(t)dt}$$

where β (t) is the property concentration at a time t ($g.m^{-3}$), Q(t) is the flow rate of water ($m^3.s^{-1}$) and t_0, t_f are the defined beginning and end of the discharge event, respectively.

2.2.6 Model implementation and calibration procedure

For MOHID Land implementation, the data described above was introduced in model interface MOHID Studio (www.actionmodulers.com) that integrates pre-processing tools, project management, model simulations and result visualization. MOHID Land uses ascii file format for input data as configuration files (with processes connected/disconnected) and time series or grid data and HDF format for time and space variant data/results.

The river sections were spatially interpolated with an automatic tool and verified against field observations. Since water level was one of the results to compare to data, the section geometry definition was of great importance. The water level sampling location is in a permanent pool (so that probe sensors were always inside water) and at the station topography has a depression that is not shown by Digital Terrain Model resolution (90m) – see Figure 3. As so, drainage network cross sections were edited accordingly in order to represent the depression and narrowing of section downstream.

MOHID Land model parameter description is shown in Table 6 and next the calibration procedure is described.

Calibrating parameters for long-term dynamics

The link between precipitation and river flow in long-term dynamics is infiltration and evapotranspiration. In MOHID Land reference evapotranspiration (ET_r) is computed based on Penamn-Monteith equation and K_c is the multiplying factor (to represent the crop distinction to well drained and homogeneous alfalfa) by ET_r to compute crop potential evapotranspiration (ET_c). There was not available information on K_c evolution against time and since the objective was to represent the long-term water budget, bibliography values were investigated. Pereira, 2004 used information on crop growth for several land uses (in Portugal) to compute standard K_c values and for the Enxoé main land uses (olive tress, pasture and annual crops) K_c values tabled ranged from 0.6 to 1.1, being an common value around 0.7-0.75. Values of K_c were tested between 0.6 and 1.0 and the best fit between MOHID Land flow and the one estimated from reservoir water balance (data from 2006 to 2009) was 0.7 that is consistent with bibliography.

Calibrating parameters for floods

From the recorded floods with automatic sampler in Enxoé (four floods, two in October 2010, one in February 2011 and one in March 2011), in general, the first peak rises observed in level field data seemed to be missing in first MOHID simulations because the precipitation water was infiltrating and was not getting to the river (Figure 6 and Figure 7). In fact it was observed that almost systematically, even for first rain events after days or weeks without precipitation, river water depth measures responded to precipitation events with similar heights as the second or third peaks (same magnitude but usually lower) whereas model simulations were at times not obtaining the first peaks. Several hypotheses were tested to check if soil properties could be causing excess infiltration but even the extreme soil conditions could not explain the first peaks (see Results and Discussion).

Results showed that Enxoé watershed soil may behave with decreased permeability, and as seen in bibliography, that may be caused by compaction, rain, fires or urban areas (Assouline, 2004). In Enxoé there were no recent fires and urban presence is low (only one village with low density). Rain may have a compact effect, destroy soil aggregates and the released material may deposit and fill soil pores reducing permeability (Assouline, 2004, Assouline and Ben-Hur, 2006) and plowed fields may also enhance soil sealing behavior by creating preferential pore orientation parallel to the soil surface (Panini et al. 1997).

Also compaction (by cattle or machinery) may change surface soil properties and all these processes may be involved in the low permeability observed in Enxoé data. The relative importance of each process lies beyond the scope of this article and thus a simple characterization of permeability loss was tested.

Deposition tends to occur in lower slopes because of reduced flow velocities and power and also plowing and cattle production is preferred in these areas (eases machinery processes, have lower soil loss, and usually are nutrient enriched areas). In general lower slopes occur in river valleys as observed in Enxoé where small depressions form. The loss of permeability was tested in the model with a varying factor accordingly to drained areas from headwaters up to reaches. An impermeabilization scenario was tested (limiting the area available for infiltration in each cell) and the best fit between simulated and data measured level for first floods was obtained with impermeabilization percentage from 5% in headwaters to 50% when reaching a river section.

The results in flood level will be presented with and without the above impermeabilization to show the impact of the procedure.

3 Results and Discussion

3.1 MOHID Land model results: comparison with field data

The comparison between MOHID Land model and field data was made in two different aspects: i) monthly inflow to the reservoir; ii) flood sampled level, in order to capture both the long-term and flood dynamics.

The graphical comparisons are presented in the next sections and resumed at the Table 1 where it can be seen that in terms of monthly flow model adjustment to data is quite satisfactory with R^2 and Nash-Sutcliff efficiencies higher than 0.85 (same trend and same order of values). For hourly levels it was obtained R^2 higher than 0.25 and Nash-Sutcliffe efficiencies higher than 0.60.

3.1.1 Monthly reservoir inflow

Input flow to the reservoir has an important role on: i) reservoir water volume and depth (water quality in small depths tends to deteriorate due to the availability of light up to the bottom); ii) retention time (with increasing retention time increasing accumulation and time for algal assimilation of nutrients) and iii) horizontal and

vertical mixing of water (intense mixing may deliver bottom nutrients to surface water with higher light and temperature availability). As so, describing the input flow from the watershed is of major importance for driving reservoir dynamics.
Enxoé watershed was an ungauged watershed and to evaluate MOHID Land model results it was used an indirect method to estimate inflow from field data: a reservoir balance was computed using volumes, discharges, precipitation and evaporation data for the period where all the components were available (January 2006 to August 2009).
The comparison between estimated inflow from reservoir balance and MOHID Land model result is shown in Figure 5 and Table 1.
Figure 5 presents on top the time series comparison between monthly flows from reservoir balance and MOHID Land model results (2006-2009); also monthly precipitation is presented in reverse axis. The same figure below shows the same values (from data and modeled) plotted in xx and yy axis. From Figure 5 can be seen that both model results and estimate from reservoir balance have the same trends (higher reservoir inflows in winter as response to precipitation and very low or zero inflows in summer with absence of rain) represented by the R^2 (0.88) and model is able to predict data values represented by NS efficiency (0.88).
The results obtained are comparable to the ones commonly present in bibliography with SWAT model as obtained in Fohrer, 2001 in two watersheds in Hesse, Germany (R^2 of 0.71 and 0.92), Geza and McCray, 2008 in a 126 km^2 Turkey Creek watershed in Denver; USA (NSE 0.61 and 0.70 and R^2 of 0.62 and 0.74) or Green and van Griensven, 2008 in small watersheds in Texas, USA (NSE from 0.59 to 0.95 and R^2 0.60 to 0.96). In Mediterranean countries Dechmi et al. 2012 in Del Reguero river a 20 km^2 watershed in northern Spain obtained high R^2 and NSE values of 0.90 while Panagopoulos et al. 2011 in Arachtos catchment (2000 km^2) in western Greece found NSE values of 0.51 to 0.68 and R^2 of 0.86-092. The present results in terms of monthly flow lie in between the bibliography satisfactory and good results, showing that MOHID Land model is able to represent at monthly scale the inflow to the reservoir

The monthly flow results above are the ones with the scenario with increased impermeabilization (see Calibration procedure) to mimic permeabilization loss evidenced in first floods data.

3.1.2 Flood level

As referred above flood rise and fall is fast in Enxoé, representative of a flushy regime what may have implications on transported material to the reservoir and on the reservoir response. The flushy regime in Enxoé induced the implementation of an automatic scheme with an automatic sampler (Figure 1 for location) connected to a multiparametric probe (sampling each 10 cm rise or fall) and four floods were collected during 2010-2011 hydrological year being shown two that are representative of i) first floods of the year (October 2010) and ii) during winter (February 2011).

Figure 6 presents on top the probe measured water depth (dots) and simulated water depths for October/November 2010 and in secondary axis in reverse order hourly precipitation is shown. Two MOHID Land simulations are presented: one with increased impermeabilization (line) to mimic permeability loss and one without (line with dots). Figure 6 shows that field data responds fast to rain events producing two level rises that took around 2-5 hours to peak and level falls around 12h as a response to two rain events of around 7 $mm.h^{-1}$.

The fast rise behavior is common in Mediterranean climate small sized watersheds as seen in Obermann et al. (2007) and Obermann et al. (2009) in Vene, France, a 67 km^2 catchment where floods were observed with 1.5h duration or Merhavia watershed with 27 km^2 and floods recorded where time to flow peak was lower than 3h (Rozaris et al. 2010).

The data first level peak in Figure 6 was preceded by almost 20 days of no rain in the watershed making possible for the soil surface to dry out. Model results for the first peak (without increased impermeability) could not represent the level rise because the head gradient in soil made infiltration possible and with a rate as rain intensity resulting in no peak in the river. This happens because evapotranspiration removes surface soil water and creates suction (negative head), generating surface head gradients that promote infiltration. The infiltration velocity obtained from Richards equation is

$$v_i = -K_{sat}\left(\frac{\partial h}{\partial z} + 1\right)$$

Where v_i is infiltration velocity, K_{sat} is saturated conductivity.

Only when surface soil is saturated (suction gradient is zero), infiltration velocity is the saturated conductivity; as evapotranspiration removes surface water higher suction occurs and infiltration velocities get higher than saturated conductivity. The process is normally seen when first rains effect is the increase of soil water content not generating surface runoff until soil is nearly saturated or heavy rains occur (James and Roulet, 2009, Li et al. 2012).

Various studies have noted the difficulty on describing the spatial and temporal variability of runoff production in arid or semi-arid areas as Michaud and Sorooshian, (1994) using KINEROS model in a 150 km^2 watershed or Al-Qurashi et al. (2008) in a 734 km^2 watershed in Oman. The main difficulties observed are associated to initial conditions (Chahinian et al. 2005), precipitation distribution, soil type, land use, or soil crusting (Al-Qurashi et al. 2008).

It was assumed that the precipitation rates were correct because for consecutive floods after soil was completely saturated and when all rain water gets in to the river, the model predicted correctly the measured level dynamics (Figure 6 and Figure 7) and model evapotranspiration was validated in the monthly flow analysis. The most extreme conditions on soil permeability were tested in the model (using clayish soils in the entire watershed or decreasing saturated conductivity to unreal vales) but still the first peaks present in Enxoé data were still missing in the model. The best land use and soil data available was used so the impermeabilization/soil crusting option was tested. Since Enxoé results on first floods cumulative load showed a behavior similar to urban watersheds (refer to next results), it reinforced the exploitation of impermeability as an option to represent the low permeability evidenced in the data. The impermeability grid used increases with drained area to mimic the possible effect of soil clogging with depositional areas, and compaction by animal farming, tillage and wheeling that generally occur preferentially in lower slopes (refer to calibration section). It is suggested that permeability loss is studied after in more detail but it falls out of the scope of the present article.

With the increased impermeabilization, in general, model was able to represent both the first and consecutive peaks water depth order and rise and fall slopes.

Figure 6 bottom shows for the same flood the hourly level from measured data and modeled, plotted in xx and yy axis with y=x line representing perfect fit and Table 1 the coefficient of determination and NSE obtained. From this figure and table the average correlation (0.27) and satisfactory NSE (0.63) shows that model was able to represent the main trends and order of magnitude of measured data.

Figure 5 presents on top the probe measured water depth (dots) and simulated water depths for February 2011 flood and in secondary axis in reverse order the precipitation. The same simulations lines are presented as before. From level measured data it can be seen, as stated in October 2010 flood, that flood rises are fast, in a couple of hours, and now flood fall takes almost a day probably being affected by higher groundwater flow as a response to high aquifer levels. In the three peaks occurred it is possible to see that model results without increased impermeabilization lack flow in the river in the first peak but in third peak both model results and data are similar. The third peak represents a situation where almost all the watershed is saturated and the fit shows that the model is representing precipitation and surface water movement accurately (runoff and river flow mainly predominant since infiltration is almost absent).

Figure 5 bottom shows for the same flood the hourly level data and modeled plotted in xx and yy axis and Table 1 the R^2 and Nash-Sutcliff efficiency (NS efficiency). From this figure and table a good agreement was obtained with R^2 of 0.83 and NS efficiency of 0.62 showing that model was able to accurate reproduce the trends and the values of measured data.

These results are comparable to the obtained in the studied floods with diverse models as described in Chahinian et al, (2005) in southern France in a 1200 m^2

watershed using four models (based on GreenAmpt, Richards equation, Horton model and Soil Conservation Service (SCS) equation) to describe 28 events where 8 had NSE higher than 0.7, Donnelly-Makowecki et al. (1999) in 60 ha watersheds in Canada with 50 events reproduced by TOPMODEL with NSE around 0.89 to 0.93 or Rozalis et al. (2010), using SCS equation for infiltration and diffuse wave for routing in a 27 km^2 watershed in Israel with maximum R^2 of 0.9 and maximum NSE of 0.83.

The increased impermeabilization was an important factor to predict first floods rise implicitly taking into account the loss of permeability needed (e.g. soil sealing, compaction, etc.) that the model does not explicitly simulate. The increased impermeabilization yielded better results in flood conditions but also created occasional summer flows as a response to precipitation that are not likely to occur in Enxoé and that suggest that the process is temporary. In the future these processes should be included in MOHID Land and integrated with detailed field work on surface soil properties to understand what are the main processes controlling permeability loss in Enxoé.

3.2 Enxoé watershed flood dynamics

The comparison between model simulation and field data showed that MOHID Land hydrology was able to represent the long-term flows and also flood level rises and falls. As so, model flow was used to compute river loads (using field data concentrations collected in Enxoé) during 2010-2011 to i) quantify the role of floods (and first floods) in annual volume and nutrient loads to the reservoir and ii) qualitatively describe the flood dynamics (and first floods) using Normalized Cumulative Loads and Discharge.

Table 7 shows the results in terms of volume and load per flood and percentage of accumulated annual value for the 4 sampled floods. Analyzing solely the Table 7 one would consider that first floods in October would not play a significant role on input to the reservoir since generate less volume (dryer soil and higher infiltration) and less load (less than 3% of annual volume and less than 7% of annual nutrient load) than February and March loads that represent 10-20% both of annual volume and nutrient load. However, as discussed in the introduction, biologic systems respond to concentration and loads are important if change downstream water body concentrations; flow controls the extent and the time that the concentration will be available. Figure 7 shows again October 2010 (top) and February 2011 (bottom) flood level but now with total nitrogen and total phosphorus concentrations during flood (automatic sampling) and previous and after flood in low waters (manual sampling). And it can be seen that in October 2010 during flood total nitrogen concentration is 5 times higher and total phosphorus 50 times higher than in low waters. However in February 2011 flood the total nitrogen and total phosphorus concentrations are very similar during flood and low waters. This is explained by the accumulation of organic matter in land and river bed during dry season that in first floods of the hydrologic year are transported downstream creating high concentration peaks (Lillebo et al. 2007, Obermann et al. 2009). With the ongoing rain events during winter floods soil surface is washed and leaching in soil has a similar effect on groundwater, being able to mobilize dissolved properties from deeper soil layers homogenizing concentrations throughout the several mediums and justify the sampled values in flood event similar to low waters value.

One curious feature also present in Figure 7 is the high total nitrogen concentrations just after the two peaks in October 2010. These concentrations correspond almost completely to nitrate and represent the arrival of groundwater (as a response to precipitation and rising aquifer level) to the river that has a delay to peaks since groundwater has a longer and slower path trough soil than surface water. The high concentrations arriving from soil may be a result of first fertilizations, mineralization of organic matter and evaporation during dry season and similar patterns of nitrate (anticlockwise hysteresis) are found in other watersheds with diverse sizes and climatic conditions (House and Warwick, 1998, Oeurng et al. 2010, Chen et al. 2012).

Other way to analyze flood dynamics is trough the use of Normalized Cumulative Load vs Normalized Cumulative Discharge. These curves were computed using suspended solids, total nitrogen, total phosphorus, nitrate (in N) and orthophosphate (in P) collected with automatic sampler during the above discussed floods (Figure 9). Figure 9 shows for the first peaks of the two floods (top October 2010 and bottom February 2011) in xx axis cumulative flow fraction and in yy axis each property cumulative load fraction. Discharge used for computation was MOHID Land model results integrated in a 5 min interval (minimum interval in concentration sampling). Results are presented in Figure 8 top for October 2010 flood and bottom for February 2011 (first peaks of each flood event). As expected suspended solids and total nitrogen and total phosphorus appear left to the bisector while dissolved properties appear in the bisector or right to it. This means that the October 2010 flood transports high amount of material (suspended particles and organic matter) that arrives to the river before the discharge peak (material deposited in the river bed and in neighbor areas inland). In the left to the bisector the suspended solids show a fast increase of load in the first moments of the flood reaching to 60% of the total load in 20% of the flood volume. Total phosphorus (in which the adsorbed components are associated to suspended solids) appears next increasing to 40% of the load in 30% of the flood volume. In the other side of the bisector is nitrate that arrives later than suspended solids and organic compounds because of its origin not associated to easy detachable particles that are transported in fast surface water but more prone to travel trough the soil (as seen in Figure 7 top that high concentrations get to the river some hours after the two flood peaks). On the other side, the February 2011 flood is shown in Figure 8 bottom where no significant difference exists between properties and all are aligned in the bisector meaning that the concentration almost maintained constant during flood (seen in Figure 7 bottom). As said previously, after the initial washing of soil surface and groundwater with first floods of the year (transporting the material accumulated during months of dry season) the winter events homogenize concentrations throughout the watershed.

Conceptually the results with the first flush effect where the main portion of the load is transported in the first moments of the flood (suspended solids, total phosphorus and total nitrogen) are throughout described in bibliography (Bertrand-Krajewski et al. 1998, Lee et al. 2002, Ribarova et al. 2008). Quantitatively these findings are also in line with bibliography as October 2010 has a first flush effect in suspended solids by the definition of Wanielista and Yousef (1993) where at least 50% of the mass is transported in 25% of the volume and very close to the definition of Bertrand-Krajewski et al. (1998) where at least 80% of the load is transported by 30% of the volume (very rare events). Obermann et al. (2009) in Vene river found FF_{25} (load fractions in 25% of flood volume) of 0.39-0.72 in suspended solids (0.69 in October 2010 flood in Enxoé), 0.38-0.61 in total phosphorus (0.35 in Enxoé) and 0.29-0.36 in total nitrogen (0.31 in Enxoé). Lee et al. (2002) and Ma et al. (2011) studied urban watersheds in South Korea and China, respectively, and October 2010 results for cumulative loads fractions in Enxoé had same order of magnitude of maximum average values in these studies. This reinforces the loss of permeability shown in first floods in Enxoé and the approach taken in modeling using increasing impermeabilization since first flood behavior is similar to the observed in urban watersheds.

A special note should be addressed for computing flood loads in these flushy regimes. In Figure 10 it is shown the total suspended solids concentration and flow (in relative values for conceptual behavior) for the first flood in October 2010. Since time to peak in floods in Enxoé is usually one hour or two (almost two in Figure 10) and in first floods the concentrations (specially suspended sediment and organic compounds) may have their peak in a question of minutes (15 minutes in Figure 10), to avoid overprediction of floods, flow should be available with at least a lower frequency than concentration variability. In the absence of automatic systems for flow measurements, only models with low time steps are able to represent this behavior and with higher steps (e.g. hourly or daily), flow will be the integration of a part or more than one flood but the high concentration used is only representative of the first minutes what may yeld overprediction in loads.

Enxoé river computed nutrient exports were of 13 tonN.year^{-1} and 1 tonP.year^{-1} resulting in around 3.7 kgN.ha^{-1}.year^{-1} and 0.3 kgP.ha^{-1}.year^{-1} consistent with similar results obtained with SWAT model implementation in Enxoé (2.5-2.8 kgN.ha^{-1}.year^{-1} and 0.3 kgP.ha^{-1}.year^{-1} in unpublished work). The nutrient export values obtained in Enxoé are in the same order as the obtained by Alvarez-Cobelas et al. (2010) using monitoring data from 3 semi-arid sub catchments in Spain with mainly vineyards and forest with annual precipitations around 400 mm and found values that ranged from 0.05 to 7 kgN.ha^{-1}.year^{-1} and from 0.0004 to 1.6 kgP.ha^{-1}.year^{-1}. High values of nitrogen export tend to occur in areas where agriculture is more nutrient intensive and annual precipitation is higher promoting nitrate leaching as, for example, Central Europe (e.g. Salvia-Castellví et al. 2005) study with field data in several Belgian watersheds found nitrate exports from around 27-33 kgN.ha^{-1}.year^{-1} in agricultural watershed with annual precipitation regimes of around 700-1200 mm). In the other end, phosphorus exports tend to be higher in areas with high erosion that can go to values of hundreds of kgP.ha^{-1} -Casasnovas (2004) in a vineyard in northeast Spain.

Enxoé results of exported nutrients to the reservoir are in the same range as bibliography results from extensive agriculture areas with gentle slopes (low erosion) and reduced human presence.

The future work in Enxoé as referred will continue applying a reservoir model that will be fed by watershed models (SWAT and MOHID Land) that may test the effect of watershed loads on reservoir and test management strategies to reduce reservoir trophic state.

4 Conclusions

The work presented was the first part of the objective to understand the origin of the high eutrophic state of Enxoé reservoir and to test management options to reduce it.

MOHID Land was applied to Enxoé and the results were compared to field data.

MOHID Land obtained satisfactory to good agreement with measured data for monthly simulated flow with R^2 of 0.88 and Nash-Sutcliffe efficiencies of 0.88 and for hourly levels was obtained R^2 higher than 0.25 and Nash-Sutcliffe efficiencies higher than 0.60.

The approach showed: i) that MOHID Land model was able to represent both long term and short term hydrodynamics of semi-arid temporary stream, and ii) first floods of the year in Enxoé may have lower weight in terms of load but transport really high suspended solids and organic matter that may have influence in reservoir primary production and oxygen consumption. The flood in October 2010 ranged in the first flush definitions in bibliography and total sediment, total nitrogen and total phosphorus transport had similar ranges observed in urban watersheds reinforcing the loss of permeability observed in first floods in Enxoé.

Flushy regimes as seen in Enxoé where flood rise may occur in one hour and concentration rise and fall in a question of minutes, the study of flood dynamics need the use of models with short time step (minutes or seconds) in order to accurately predict loads. MOHID Land being a continuous, variable time step and physically based model showed to be suited for describing the both the short-term (flood) and long-term dynamics (monthly and yearly) occurring in flushy Mediterranean environments.

It was found that in Enxoé permeability loss was observed during first floods and the associated processes should be investigated to quantify the origin of the reduced permeability.

Enxoé results of exported nutrients to the reservoir are in the same range as bibliography results from extensive agriculture areas with gentle slopes (low erosion) and reduced human presence. This is a first step in conjunction to the implementation of SWAT model to characterize watershed input to the reservoir.

In the future the watershed inputs will be linked to a reservoir model and after validation of the approach with field data in the reservoir wall, management strategies will be tested to reduce reservoir trophic state.

Acknowledgments

The present work was supported within the framework of the EU Interreg SUDOE IVB program (SOE1/P2/F146 AguaFlash project), the Mirage Project (EU-FP7) and the EUTROPHOS Project (PTDC/AGR-AAM/098100/2008) of the Fundação para a Ciência e a Tecnologia (FCT).

References

Abbott, M.B.; Bathurst, J.C.; Cunge, J.A.; O'Conncll, P.E.; Rasmussen, J. (1986a) - An introduction to the European hydrological system - Système Hydrologique Européen "SHE". 1: History and philosophy of a physically based distributed modelling system. J. Hydrol. 87,45-59.

Abbott, M.B.; Bathurst, J.C.; Cunge, J.A.; O'Conncll, P.E.; Rasmussen, J.. (1986b) - An introduction to the European hydrological system — Système Hydrologique Européen "SHE". 2: Structure of a physically based distributed modelling system. J. Hydrol. 87, 61-77.

Al-Qurashi, A.; McIntyre, M.; Wheater, H.; Unkrich, C. (2008) - Application of the Kineros2 rainfall–runoff model to an arid catchment in Oman, Journal of Hydrology, Volume 355, Issues 1–4, 20 June 2008, Pages 91-105, ISSN 0022-1694, 10.1016/j.jhydrol.2008.03.022.

Alvarez-Cobelas, M.; Sánchez-Andrés, R.; Sánchez-Carrillo, S.; Angeler, D.G. (2010) - Nutrient contents and export from streams in semiarid catchments of central Spain. Journal of Arid Environments, Volume 74, Issue 8, August 2010, Pages 933–945

ASCE (1996) - Hydrology Handbook, American Society of Civil Engineers, Task Comitee on Hydrology Handbook, II Series. GB 661.2.H93. 1996. 96-41049.

Assouline, S.; Ben-Hur, M. (2006) - Effects of rainfall intensity and slope gradient on the dynamics of interrill erosion during soil surface sealing. Catena 66 (2006) 211 – 220.

Assouline, S. (2004) - Rainfall-Induced Soil Surface Sealing: A Critical Review of Observations, Conceptual Models, and Solutions. Vadose Zone Journal 3:570–591 (2004). Soil Science Society of America.

Brito, D.; Neves, R.; Branco, M.A.; Prazeres, A.; Rodrigues, S.; Gonçalves, M.C.; Ramos, T.B. () – Assesing long-term dynamics and nutrient loads to an eutrophic reservoir in a temporary river basin in southeast Portugal (Enxoé). Submitted to Journal of Hidrology.

Bailly, D.; Brito, D.; Oeurng, C.; Neves, R.; Sauvage, S.; Sánchez-Pérez, J.-M. (2010) - Assessment of suspended matter transport in a large agricultural catchment using the MOHID water modelling system. EGU General Assembly 2010, 2-7 May, 2010 in Vienna, Austria, p.12343.

Barão, L.; Chambel-Leitão, P.; Braunschweig, F.; Neves, R.J.; Gonçalves, M.C.; Ramos, T.B.; Castanheira, N.L. (2010) - Simulation of water dynamics in two irrigated soils. Rev. de Ciências Agrárias v.33 n.1 Lisboa jan. 2010.

Bertrand-Krajewski, J-L; Chebbo, G.; Saget, A. (1998) - Distribution of pollutant mass vs volume in stormwater discharges and the first flush phenomenon, Water Research, Volume 32, Issue 8, August 1998, Pages 2341-2356, ISSN 0043-1354, 10.1016/S0043-1354(97)00420-X.

Bicknell, B.R., Imhoff, J. C.; Kittle, J. L.; Donigian, A. S; Johanson, R.C. (1993) - Hydrological Simulation Program - FORTRAN (HSPF): Users Manual for Release 10. EPA-600/R-93/174, U.S. EPA, Athens, GA, 30605.

Boughton, W.; Droop, O. (2003) - Continuous simulation for design flood estimation—a review. Environmental Modelling & Software 18 (2003) 309–318.

Boutron, O.; Got, P.; Caro, A; Salles, C.; Perrin, J.-L.; Rodier, C.; Marchand, P.; David, A.; Neves, R.; Tournoud, M.-G. (2010) - Modelling faecal coliforms and streptococci dynamics in an intermittent French river with Mohid River Network. EGU General Assembly 2010, 2-7 May, 2010 in Vienna, Austria, p.13721

Brunner, G.W. (2010) - HEC-RAS River Analysis System User’s Manual ver. 4.1

Carlson, R. E., (1977) - A trophic state index for lakes. Limnology and Oceanography, 22: 361-369.

Chahinian, N.; Moussa, R.; Andrieux, P.; Voltz, M. (2005) - Comparison of infiltration models to simulate flood events at the field scale, Journal of Hydrology, Volume 306, Issues 1–4, 9 May 2005, Pages 191-214, ISSN 0022-1694, 10.1016/j.jhydrol.2004.09.009.

Chen, N.; Wu, J.; Hong, H. (2012) - Effect of storm events on riverine nitrogen dynamics in a subtropical watershed, southeastern China, Science of The Total Environment, Volume 431, 1 August 2012, Pages 357-365, ISSN 0048-9697, 10.1016/j.scitotenv.2012.05.072.

Dechmi, F. Burguete, J. Skhiri, A. (2012) - SWAT application in intensive irrigation systems: Model modification, calibration and validation, In Press - Journal of Hydrology, Volumes 470–471, 12 November 2012, Pages 227-238, ISSN 0022-1694, 10.1016/j.jhydrol.2012.08.055.

Donnelly-Makowecki, L.M.; Moore,R.D. (1999) - Hierarchical testing of three rainfall–runoff models in small forested catchments, Journal of Hydrology, Volume 219, Issues 3–4, 8 July 1999, Pages 136-152, ISSN 0022-1694, 10.1016/S0022-1694(99)00056-6.

Debele, B.; Srinivasan, R.; Parlange, J.-Y. (2005) - Coupling upland watershed and downstream waterbody hydrodynamic and water quality models (SWAT and CE-QUAL-W2) for better water resources management in complex river basins. Springer Science + Business Media B.V. 2006.

Esteves, M.; Faucher, X.; Galle, S.; Vauclin, M. (2000) - Overland flow and infiltration modelling for small plots during unsteady rain: numerical results versus observed values, Journal of Hudrology 228 (2000) 265-282

Feddes, R.A.; Hoff, H.; Bruen, M.; Dawson, T.; de Rosnay, P.; Dirmeyer, P.; Jackson, R.B.; Kabat, P.; Kleidon, A.; Lilly, A.; Pitman, A.J. (2011) - Modeling Root Water Uptake in Hydrological and Climate Models. Bulletin of the American Meteorological Society 2001;82:2797-2809

Fohrer, N; Eckhardt, K.; Haverkamp, S.; Frede, H.G. (2001). Applying the SWAT Model as a Decision Support Tool for Land Use Concepts in Peripheral Regions in Germany. Pages 994-999 Sustaining Global Farm. Papers from the 10th International Soil Conservation Organisation Meeting.

Geza, M.; McCray, J.E.(2008) - Effects of soil data resolution on SWAT model stream flow and water quality predictions, Journal of Environmental Management, Volume 88, Issue 3, August 2008, Pages 393-406, ISSN 0301-4797, 10.1016/j.jenvman.2007.03.016.

Green, C.H.; van Griensven, A. (2008) - Autocalibration in hydrologic modeling: Using SWAT2005 in small-scale watersheds. Environmental Modelling & Software 23 (2008) 422e434

Gaßmann, M.; Friedler, E.; Dubwoski, Y.; Dinerman, E.; Olsson, O.; Bauer, M (2009) - Pesticides in the Lake Kinneret basin: a combined approach towards mircopollutant management. EGU General Assembly 2009, 19-24 April, 2009 in Vienna, Austria, p.4751.

Havens, K. E.; James, R. T.; East, T. L.; Smith, V. H. (2003) – N:P ratios, light limitation, and cyanobacterial dominance in a subtropical lake impacted by non-point source nutrient pollution. Environmental Pollution vol 122 pp 379-390.

Havnø, K.; Madsen, M.N.; Dørge, J.; (1995) - MIKE 11 - A generalised river modelling package, in Computer Models of Watershed Hydrology, Singh, V.P., Ed., Water Resources Publications, Colorado, USA, 1995, p809-846.

House, W.A.; Warwick, M.S. (1998) - Hysteresis of the solute concentration/discharge relationship in rivers during storms, Water Research, Volume 32, Issue 8, August 1998, Pages 2279-2290, ISSN 0043-1354, 10.1016/S0043-1354(97)00473-9.

Hsu, M.H.; Chen, S.H.; Chang, T.J. (2000) - Inundation simulation for urban drainage basin with storm sewer system. Journal of Hydrology volume 234 (2000) pages 21–37.

INAG (2011) – Management of the trophic status in Portuguese reservoirs. Unpublished.

INAG (2004) – Plano de Ordenamento da Albufeira do Enxoé, estudos de caracterização e pré-proposta de ordenamento. Management Plan for Enxoé Reservoir (portuguese).

James, A.L., Roulet, N.T. (2009) - Antecedent moisture conditions and catchment morphology as controls on spatial patterns of runoff generation in small forest catchments. Journal of Hydrology, volume 377 (2009), pages 351–366.

Jury, W.A.; Gardner, W.R.; Gardner, W.H. (1991) - Soil physiscs. 5th Edition 328pp. John Wiley & Sons. ISBN: 0471831085, 9780471831082.

Lee, J.H.; Bang, K.W.; Ketchum Jr., L.H.; Choe, J.S.; Yu, M.J. (2002) - First flush analysis of urban storm runoff, Science of The Total Environment, Volume 293, Issues 1–3, 3 July 2002, Pages 163-175, ISSN 0048-9697, 10.1016/S0048-9697(02)00006-2.

Li, Y.X.; Tullberg, J.N.; Freebairn, D.M.; Li, H.W. (2009) - Functional relationships between soil water infiltration and wheeling and rainfall energy, Soil and Tillage Research, Volume 104, Issue 1, June 2009, Pages 156-163, ISSN 0167-1987, 10.1016/j.still.2008.10.023.

Li, H.; Sivapalan, M.; Tian, F. (2012) - Comparative diagnostic analysis of runoff generation processes in Oklahoma DMIP2 basins: The Blue River and the Illinois River. Journal of Hydrology volume 418–419 (2012) pages 90–109

Ma, Z.-B.; Ni, H.-G.; Zeng, H.; Wei, J.-B. (2011) - Function formula for first flush analysis in mixed watersheds: A comparison of power and polynomial methods, Journal of Hydrology, Volume 402, Issues 3–4, 25 May 2011, Pages 333-339, ISSN 0022-1694, 10.1016/j.jhydrol.2011.03.029.

Michaud, J.; Sorooshian, S. (1994) - Comparison of simple versus complex distributed runoff models on a midsized semiarid watershed WATER RESOURCES RESEARCH, VOL. 30, NO. 3, P. 593, 1994

Moriasi, D.N.; Arnold, J.G.: Van Liew, M.W.; Bingner, R.L.; Harmel, R.D.; Veith, T.L. (2007) - Model evaluation guidelines for systematic quantification of accuracy in watershed simulations. Trans. ASABE 50 (3), 885–900.

Neitsch, S.L., Arnold, J.G., Kiniry, J.R., Srinivasan, R., Williams, J.R., (2002) - Soil and Water Assessment Tool. User´s Manual. Version 2005. GSWRL Report 02-02, BRC Report 2-06, Temple, Texas, USA.

Niehoff, D.; Fritscha, U.; Bronstert, A. (2002) - Land-use impacts on storm-runoff generation: scenarios of land-use change and simulation of hydrological response in a meso-scale catchment in SW-Germany. Journal of Hydrology volume 267 (2002), pages 80–93.

Obermann, M.; Froebrich, J.; Perrin, J.-L. Tournoud, M.-J. (2007) - Impact of significant floods on the annual load in an agricultural catchment in the mediterranean, Journal of Hydrology, Volume 334, Issues 1–2, 20 February 2007, Pages 99-108, ISSN 0022-1694, 10.1016/j.jhydrol.2006.09.029.

Obermann, M.; Rosenwinkel, K.H.; Tournoud, M.G. (2009) - Investigation of first flushes in a medium-sized mediterranean catchment. Journal of Hydrology volume 373 (2009) pages 405–415.

Oeurng, C.; Sauvage, S.; Sánchez-Pérez, J.M. (2010) - Temporal variability of nitrate transport through hydrological response during flood events within a large agricultural catchment in south-west France, Science of The Total Environment, Volume 409, Issue 1, 1 December 2010, Pages 140-149, ISSN 0048-9697, 10.1016/j.scitotenv.2010.09.006.

OSPAR. (2001) - Draft Common Assessment Criteria and their Application within the Comprehensive Procedure of the Common Procedure. Meeting of the Eutrophication Task Group, London, 9 -11 October 2001, Annex5. Ospar Convention for the Protection of the Marine Environment of the North-East Atlantic.

Paerl, H. W.; Fulton, R.S.; Moisander, P.H.; Dyble, J. (2001) – Harmful freshwater algal blooms: with an emphasis on cyanobacteria. The Scientific World journal. Vol 1: 76-113.

Panagopoulos, Y.; Makropoulos, C.; Mimikou, M. (2011) - Reducing surface water pollution through the assessment of the cost-effectiveness of BMPs at different spatial scales, Journal of Environmental Management Volume 92, Issue 10, October 2011, Pages 2823–2835

Ramos, M. C.; Nacci, S.; Pla, I. (2000) - Soil sealing and its influence on erosion rates for some soils in the Mediterranean area. Soil Science 2000 Vol. 165 No. 5 pp. 398-403.

-Casasnovas, J.A. (2004) - Nutrient losses from a vineyard soil in Northeastern Spain caused by an extraordinary rainfall event. CATENA, Volume 55, Issue 1, 5 January 2004, Pages 79–90

Ribarova, I.; Ninov, P.; Cooper, D. (2008) - Modeling nutrient pollution during a first flood event using HSPF software: Iskar River case study, Bulgaria. Short Communication. Ecological Modelling 211 (2008) 241–246.

Ritchie, J.T. (1972) - Model for predicting evaporation from a row crop with incomplete cover, Water Resour. Res., 8(5), 1204-1213, 1972.

Rozalis, S.; Morin, E.; Yair, Y.; Price, C. (2010) Flash flood prediction using an uncalibrated hydrological model and radar rainfall data in a Mediterranean watershed under changing hydrological conditions, Journal of Hydrology, Volume 394, Issues 1–2, 17 November 2010, Pages 245-255, ISSN 0022-1694, 10.1016/j.jhydrol.2010.03.021.

Sansalone, J.J.; Cristina, C.M. (2004) - First flush concepts for suspended and dissolved solids in small impervious watersheds. Journal of Environmental Engineering – ASCE 130 (11), 1301–1314.

Singer, M.J.; Le Bissonnais, Y. (1998) - Importance of surface sealing in the erosion of some soils from a mediterranean climate. Geomorphology 24 1998.79–85.

Panini, T.; Torri, D.; Pellegrini, S.Pagliai, M.; Salvador Sanchis, M.P. (1997) - A theoretical approach to soil porosity and sealing development using simulated rainstorms. Catena 31 (1997) 199-218

Pereira, L.S. (2004) - Necessidades de Água e Métodos de Rega. Book Europa-América, 2004 Pp.: 316. ISBN: 978-972-1-05427-1

Salvia-Castellví, M.; Iffly, J.F.; Borght, P.V.; Hoffmann, L. (2005) - Dissolved and particulate nutrient export from rural catchments: A case study from Luxembourg. Science of The Total Environment, Volume 344, Issues 1–3, 15 May 2005, Pages 51–65

Saxton, K.E. et al. (1986) - Estimating generalized soil-water characteristics from texture. Soil Sci. Soc. Amer. J. 50(4):1031-1036

Thompson, J.R.; Sørensonb, H.R.; Gavina, H.; Refsgaard, A. (2004) - Application of the coupled MIKE SHE/MIKE 11 modelling system to a lowland wet grassland in southeast England Journal of Hydrology volume 293 (2004) pages 151–179.

Trancoso, A.R., Braunschweig, F., Chambel-Leitão, P., Obermann, M. and Neves, R.(2009). An advanced modeling tool for simulating complex river systems. Science of the Total Environment volume 407, 3004-3016.

UNL. (2003) - Estudo de Avaliação das Contribuições de Águas Residuais Urbanas nas Albufeiras do Pocinho, Pracana, Maranhão e Vale do Gaio. Estudo Realizado no Âmbito do Processo de Designação de Zonas Sensíveis em Águas Superficiais, Directiva do Conselho 91/676/CEE, de 12 de Junho. Universidade Nova de Lisboa. 47 pp.

U.S. EPA. (2000) - Eutrophication from Agricultural Sources: Seasonal Patterns & Effects of Phosphorus. Final

Valério, E.; Pereira, P.; Saker, M.L.; Franca, S.; Tenreiro, R. (2005) - Molecular characterization of Cylindrospermopsis raciborskii strains isolated from Portuguese freshwaters, Harmful Algae, Volume 4, Issue 6, November 2005, Pages 1044-1052, ISSN 1568-9883, 10.1016/j.hal.2005.03.002.

Vollenweider, R.A. (1976) - Advances in defining critical loading levels for phosphorus in lake eutrophication. Memorie dell'Istituto Italiano di Idrobiologia, Vol 33: 53–83

Wanielista, M.P.; Yousef, Y.A. (1993) - Stormwater management. John Wiley and Sons, Inc, NY, USA (1993)

Woolhiser, D.A., Smith, R.E. Goodrich, D.C. (1990) - KINEROS, A Kinematic Runoff and Erosion Model: Documentation and User Manual. U S. Department of Agricultural Research Service, ARS-77, 130 p.

Yevenes, M.A.; Mannaerts, C. M. (2011) - Seasonal and land use impacts on the nitrate budget and export of a mesoscale catchment in Southern Portugal, Agricultural Water Management, Volume 102, Issue 1, 15 December 2011, Pages 54-65, ISSN 0378-3774, 10.1016/j.agwat.2011.10.006.

Table 1. Comparison of Mohid Land model results to collected data.

Parameter	Period	Data average	Model Average	RMSE	R^2	Nash-Sutcliffe Efficiency
Monthly Flow						
Monthly Reservoir Inflow	1996-2009	0.20 $hm^3.month^{-1}$	0.24 $hm^3.month^{-1}$	0.15 $hm^3.month^{-1}$	0.88	0.88
Hourly Flood Water Depth						
October 2010 Flood	28Oct-31Oct	0.50 m	0. 59 m	0.22 m	0.27	0.63
February 2011 Flood	13 Feb-18Feb	0.86 87 m	0.79 m	0.17 m	0.70	0.62

Table 2. Description of data for Mohid Land model implementation

Data type	Description	Origin	Resolution	Period	Frequency
DTM	SRTM Digital Elevation	NASA	90m	-	-
Land Use	Corine Land Cover 2000	EEA	1:100000	1999-2002	-
Soil Texture	European Soil database	JRC, EU	1:1000000	- 1996	-
Precipitation	Stations for hourly input	SNIRH, National Water Institute (www.snirh.pt/)	-	1980-2011	hourly
Other Meteorology	Stations for hourly input	SNIRH, National Water Institute (www.snirh.pt/)	-	1980-2011	hourly

Table 3. Enxoé land use distribution areas (Source: Corine 2000).

Land Use	Area (km^2)	Percentage of total area
Olive trees	21	35%
Annual crops – Rotation 2	18	30%
Pasture/“Montado”	11	19%
Forest	7	11%
Annual crops – Rotation 1	2	3%
Water	1	2%
Urban area	<1	<1%
Total	61	100%

Table 4. Enxoé land uses agricultural practices definition. Information collected from farmer questionnaires.

Agricultural Practice	Crop Wheat and Barley	Oats	Sunflower	Olive Trees
Planting	November	October	April	-
Fertilization	November 20 kgN/ha November 18 kgP/ha January 50 kgN/ha February 20 kgN/ha	March 40-80 kgN/ha	April 22 kgP/ha	April to July (24-60 kgN/ha)
Harvest	June	June	September	-

Table 5. Description of data for Mohid Land model validation.

Data type	Station	Origin	Period	Frequency
Monthly Reservoir Inflow				
Reservoir Discharges	Enxoé Reservoir (26M/01A)	SNIRH, National Water Institute	2005-2009	Monthly
Precipitation	Herdade da Valada (26M/01C), Sobral Adiça (25N/01UG)	SNIRH, National Water Institute	1980-2011	Daily
Evaporation	Herdade da Valada (26M/01C), Monte da Torre	SNIRH, National Water Institute	2001-2011	Daily
Flood level				
Water depth	Probe installed that measures water depth and collects samples during flood rise and fall	Project	2010-2011	15 min

Table 6. MOHID Land model parameter description.

Parameter Description	Variability	Values	Reference
Manning-Strickler's roughness coefficient	From Land Use map and river bed material	0.01 to 0.3	Panday and Huyakorn, 2004; Beeson et al. 2001
Impermeable Area (%)	From Land Use Map; calibration parameter for floods	5-50%	estimated
Evapotranspiration Coefficient – Kc (-)	Constant	0.7	Pereira, L.S. 2004
Feddes vegetation stress heads (m)	From Land Use map	-0.01 to -30	Feddes et al. 2001
Soil van Genuchten hydraulic parameters	From Soil map (textures) using pedotransfer functions	-	Saxton, 2006

Table 7. Flood weight on Enxoé anual flow and loads.

Flood	days*	Flood Volume (hm^3)	Fraction of Annual Volume (%)	Fraction of Annual SST Load (%)	Fraction of Annual TotalN Load (%)	Fraction of Annual TotalP Load (%)
29-31Oct2010	3	0.05	2	8	3	7
13-18Feb2011	6	0.2	9	23	9	12

* from flood start up to low waters

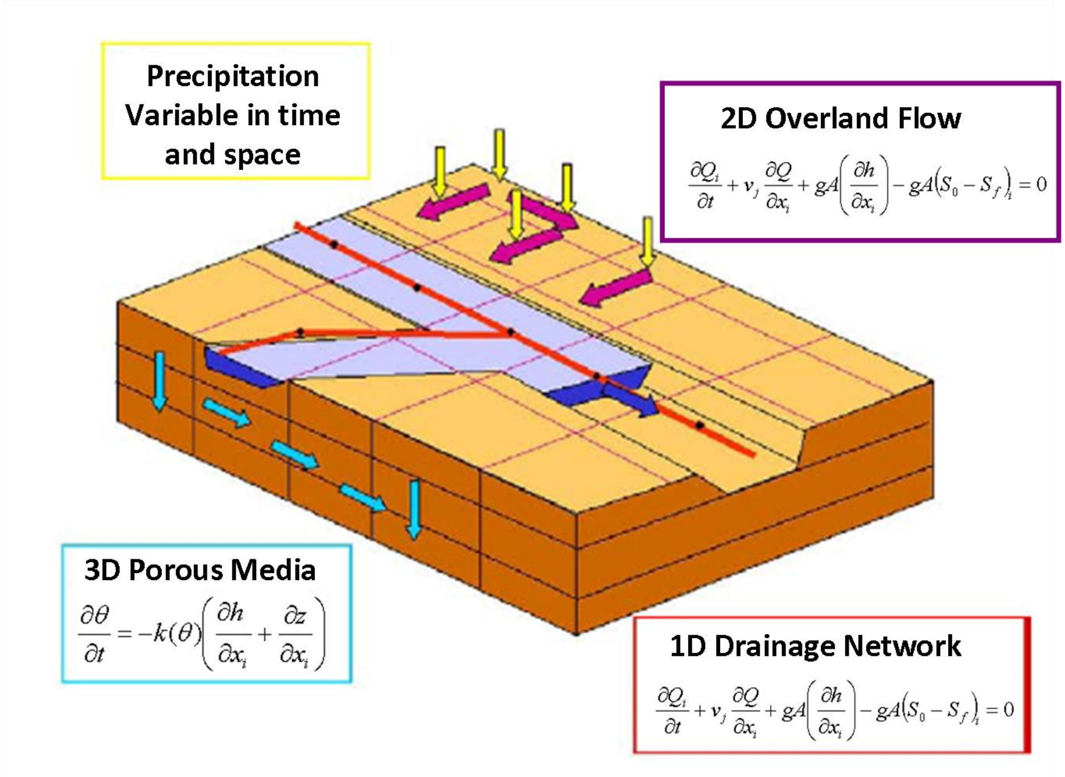

Figure 1. Mohid Land Geometry and equations.

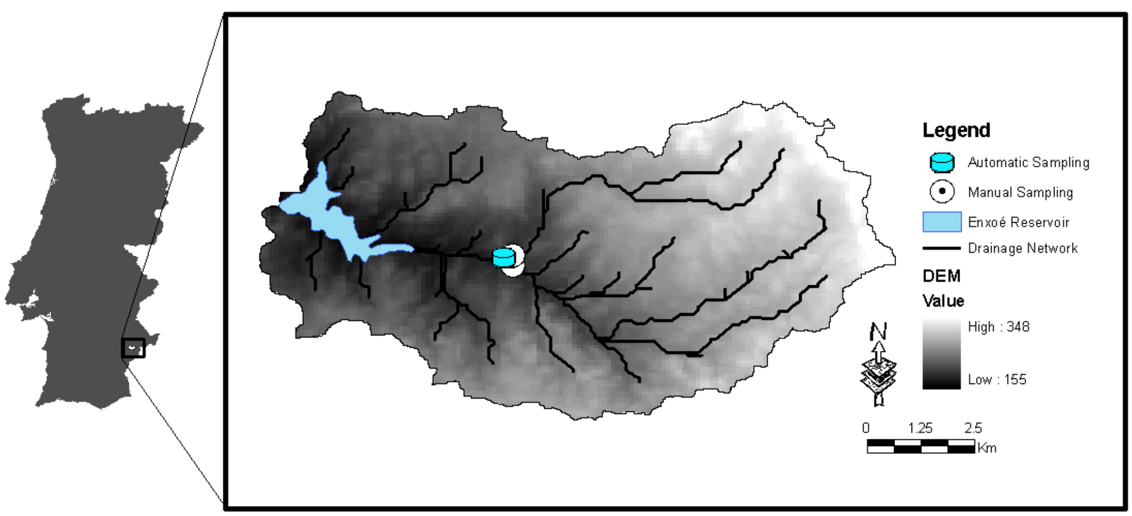

Figure 2. Location of study area and monitoring stations. Digital Elevation Model (Source: NASA) and drainage network are also displayed

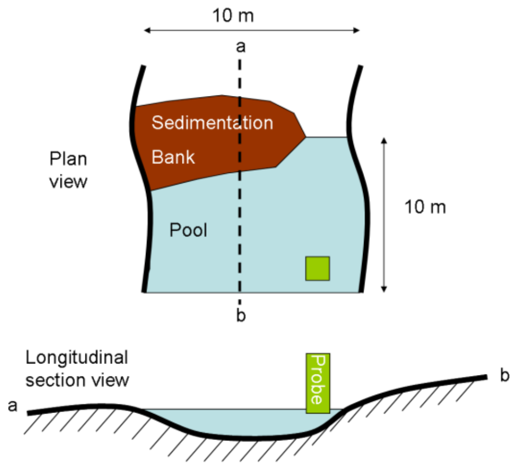

Figure 3. Automatic sampling location cross section definition.

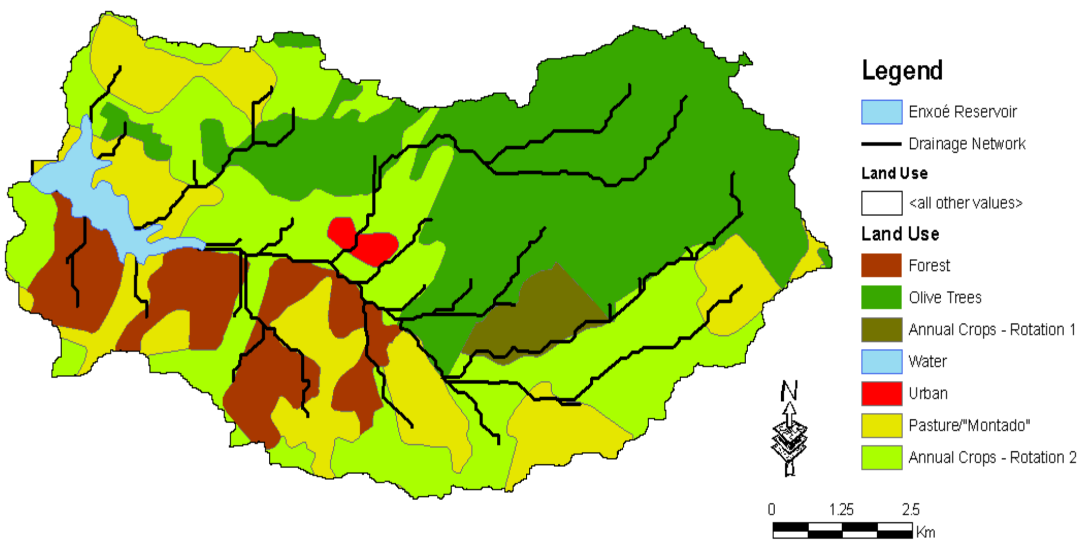

Figure 4. Enxoé land use distribution map (Source: Corine 2000). Also Enxoé Reservoir and drainage network is presented.

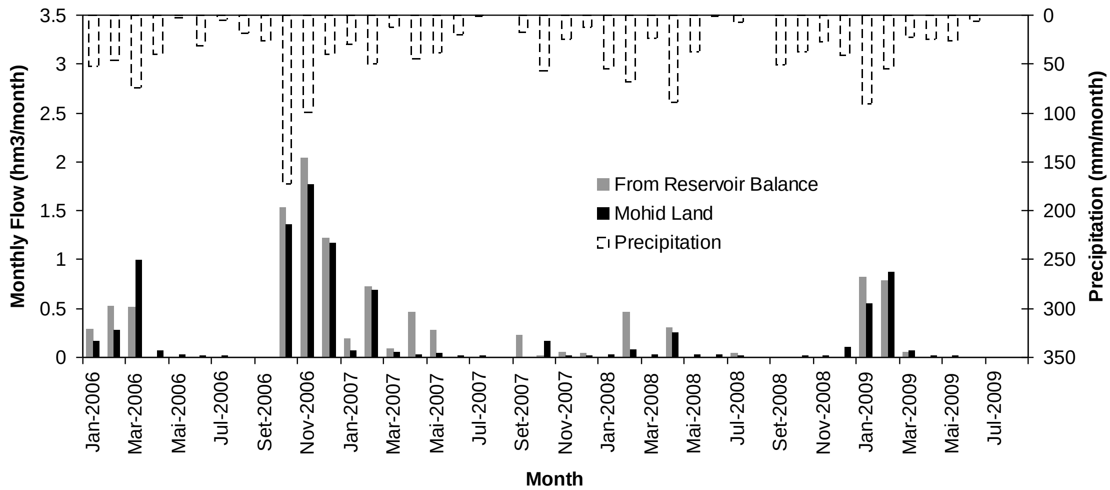

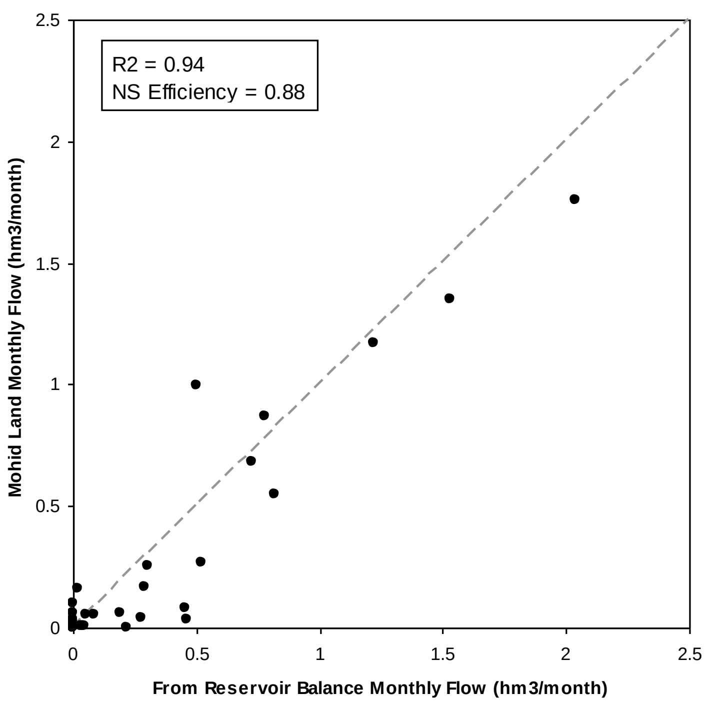

Figure 5. Monthly inflow to Enxoé reservoir - comparison between estimate from reservoir balance and simulated from MOHID Land model. Top – flow comparison per month; monthly precipitation is also presented in inverted secondary axis. Bottom – flow comparison on both axis (R^2 and Nash-Sutcliffe efficiency are indicated).

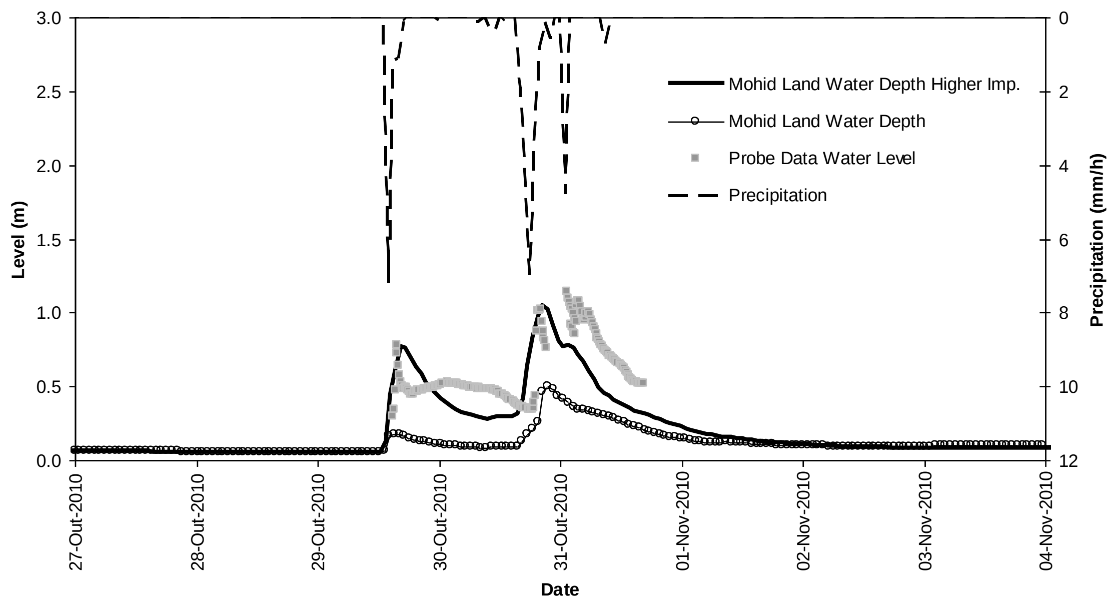

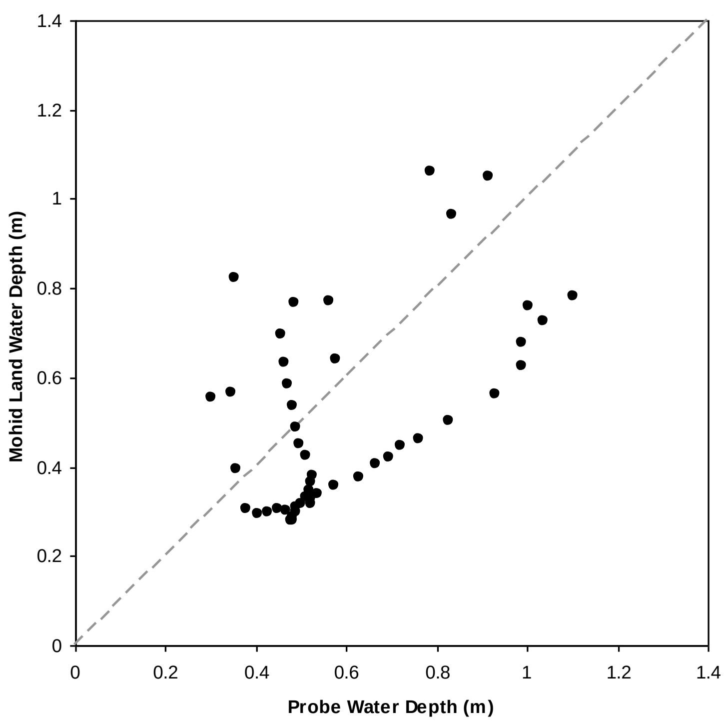

Figure 6. Top - Enxoé river hourly measured water depth versus MOHID Land model water depth during flood in October 2010; Hourly precipitation is presented in inverted seconday axis. Bottom – water depth comparison on both axis (R^2 and Nash-Sutcliffe efficiency are indicated).

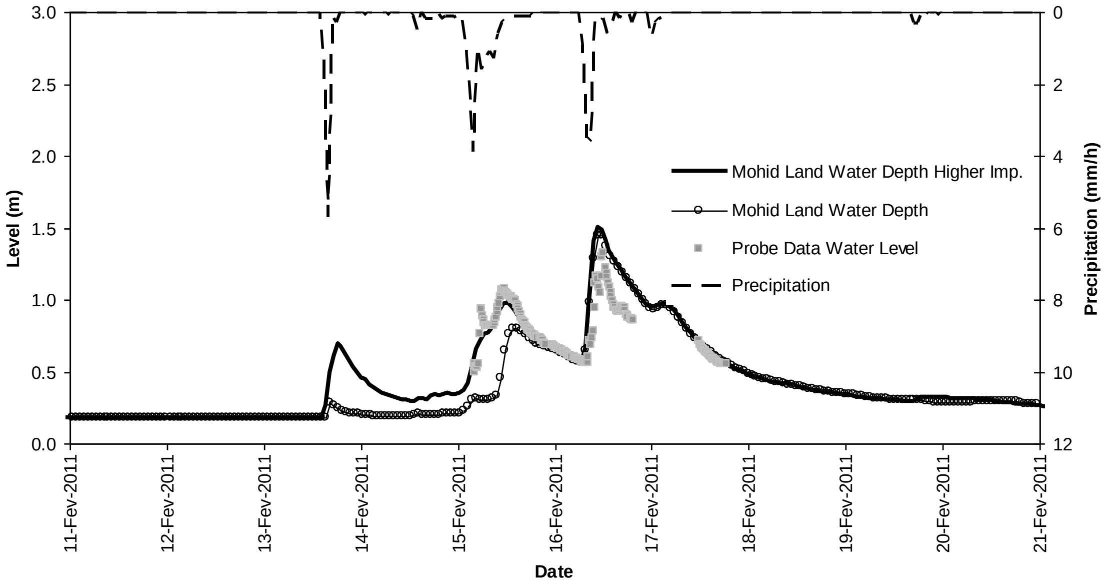

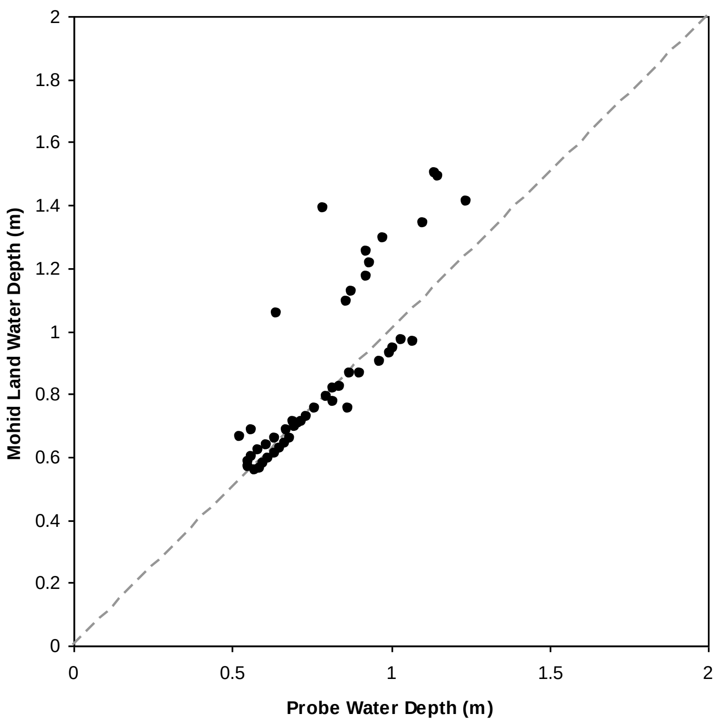

Figure 7. Top - Enxoé river hourly measured water depth versus MOHID Land model water depth during flood in February 2010; Hourly precipitation is presented in inverted seconday axis. Bottom – water depth comparison on both axis (R^2 and Nash-Sutcliffe efficiency are indicated).

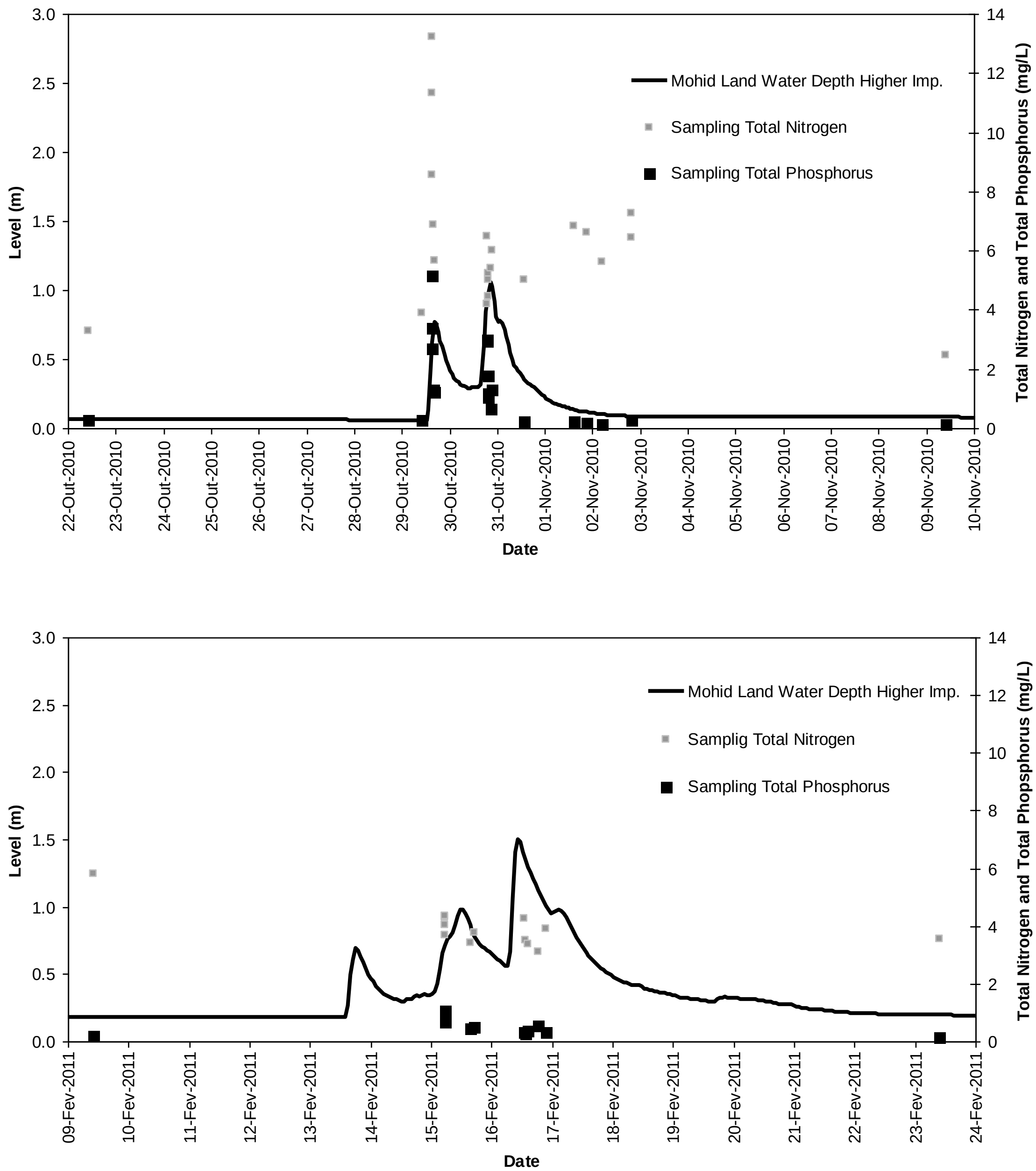

Figure 8. Top - Enxoé river total nitrogen and total phosphorus concentrations previous, during and after the flood of October 2010. Bottom - Enxoé river total nitrogen and total phosphorus concentrations previous, during and after the flood of Februay 2011.

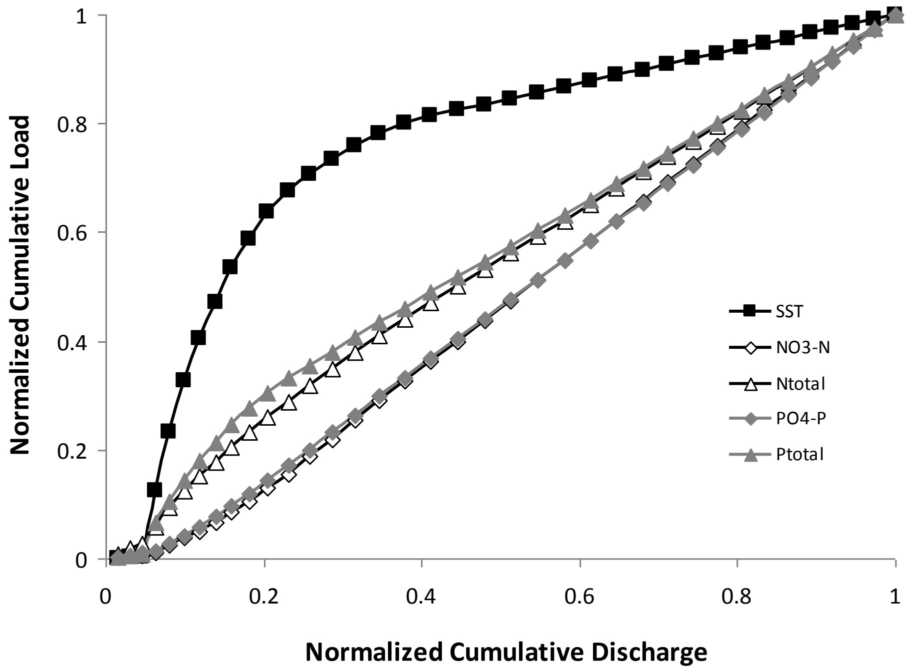

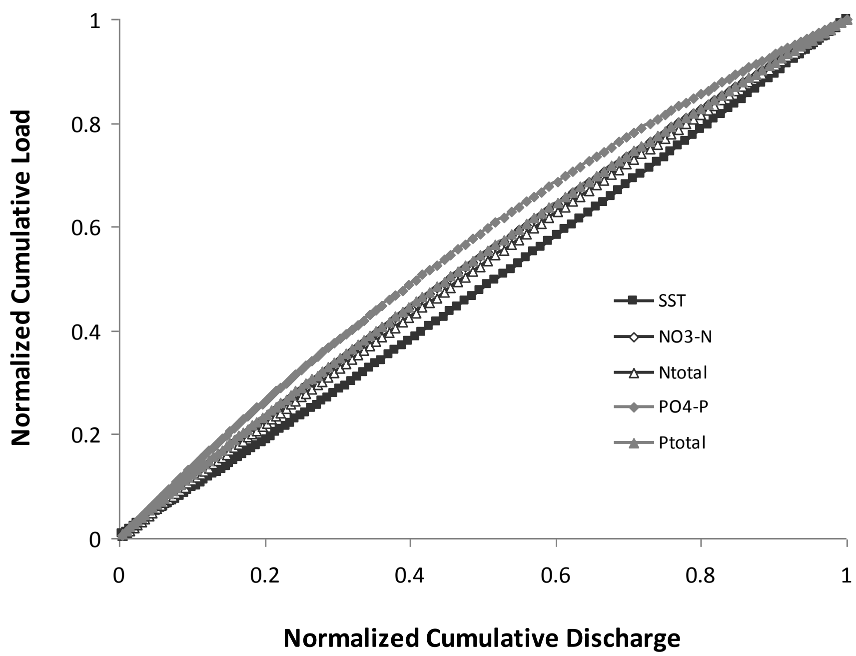

Figure 9. Enxoé river total suspended solids (TSS), total nitrogen (Ntotal), nitrate (NO3-N), total phosphorus (Ptotal) and orthophosphate (PO4-P) normalized cumulative loads versus normalized cumulative discharge. Top – for first peak in October 2010 flood and Bottom – for first peak Februay 2011 flood.

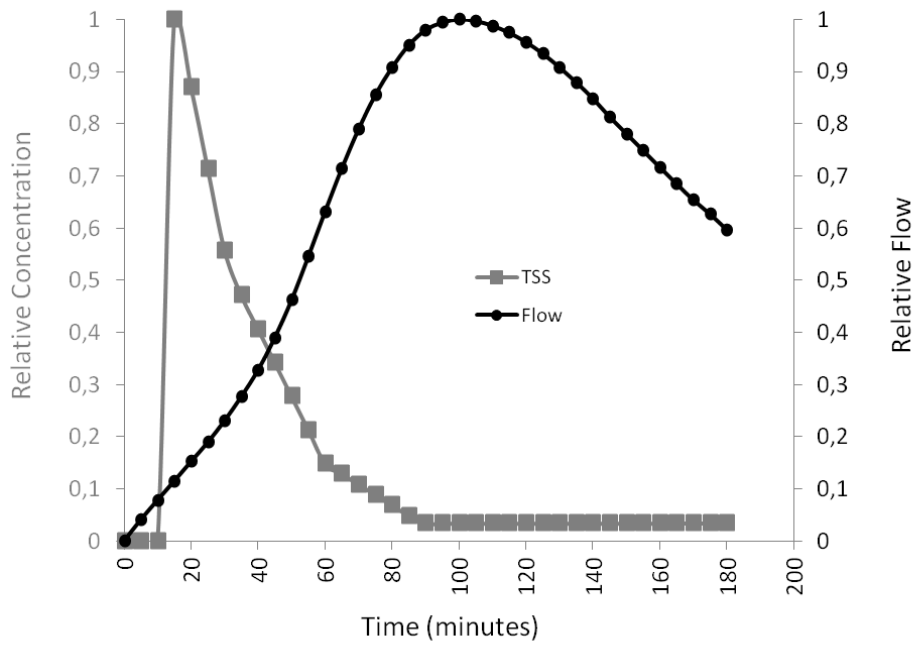

Figure 10. Enxoé river total suspended solids (TSS) relative concentration and relative flow (1 for maximum and 0 for minimum during event) for first peak in October 2010 flood.

Highlights:

- Applied MOHID Land to quantify flood role on annual loads to an eutrophic reservoir.
- MOHID Land adjusted well to monthly reservoir input flow and flood measured level.
- Reduced permeabilization was found important factor to capture first floods.
- First floods transported lower load but higher concentrations to the reservoir.

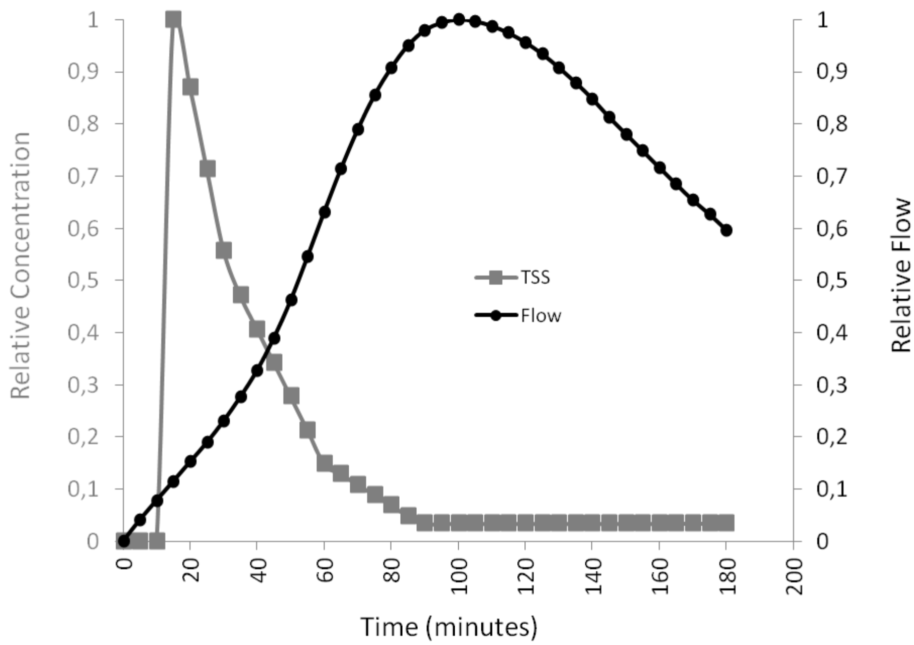

Figure 1. Enxoé river total suspended solids (TSS) relative concentration and relative flow (1 for maximum and 0 for minimum during event) for first peak in October 2010 flood.

Figure 1. Mohid Land Geometry and equations.

Figure 2. Automatic sampling location cross section definition.

Figure 3. Location of study area and monitoring stations. Digital Elevation Model (Source: NASA) and drainage network are also displayed

Figure 4. Enxoé land use distribution map (Source: Corine 2000). Also Enxoé Reservoir and drainage network is presented.

Figure 5. Monthly inflow to Enxoé reservoir - comparison between estimate from reservoir balance and simulated from MOHID Land model. Top – flow comparison per month; monthly precipitation is also presented in inverted secondary axis. Bottom – flow comparison on both axis (R^2 and Nash-Sutcliffe efficiency are indicated).

Figure 6. Top - Enxoé river hourly measured water depth versus MOHID Land model water depth during flood in October 2010; Hourly precipitation is presented in inverted seconday axis. Bottom – water depth comparison on both axis (R^2 and Nash-Sutcliffe efficiency are indicated).

Figure 7. Top - Enxoé river hourly measured water depth versus MOHID Land model water depth during flood in February 2010; Hourly precipitation is presented in inverted seconday axis. Bottom – water depth comparison on both axis (R^2 and Nash-Sutcliffe efficiency are indicated).

Figure 8. Top - Enxoé river total nitrogen and total phosphorus concentrations previous, during and after the flood of October 2010. Bottom - Enxoé river total nitrogen and total phosphorus concentrations previous, during and after the flood of Februay 2011.

Figure 9. Enxoé river total suspended solids (TSS), total nitrogen (Ntotal), nitrate (NO3-N), total phosphorus (Ptotal) and orthophosphate (PO4-P) normalized cumulative loads versus normalized cumulative discharge. Top – for first peak in October 2010 flood and Bottom – for first peak Februay 2011 flood.

Figure 10. Enxoé river total suspended solids (TSS) relative concentration and relative flow (1 for maximum and 0 for minimum during event) for first peak in October 2010 flood.

Figure1.tif
Click here to download high resolution image

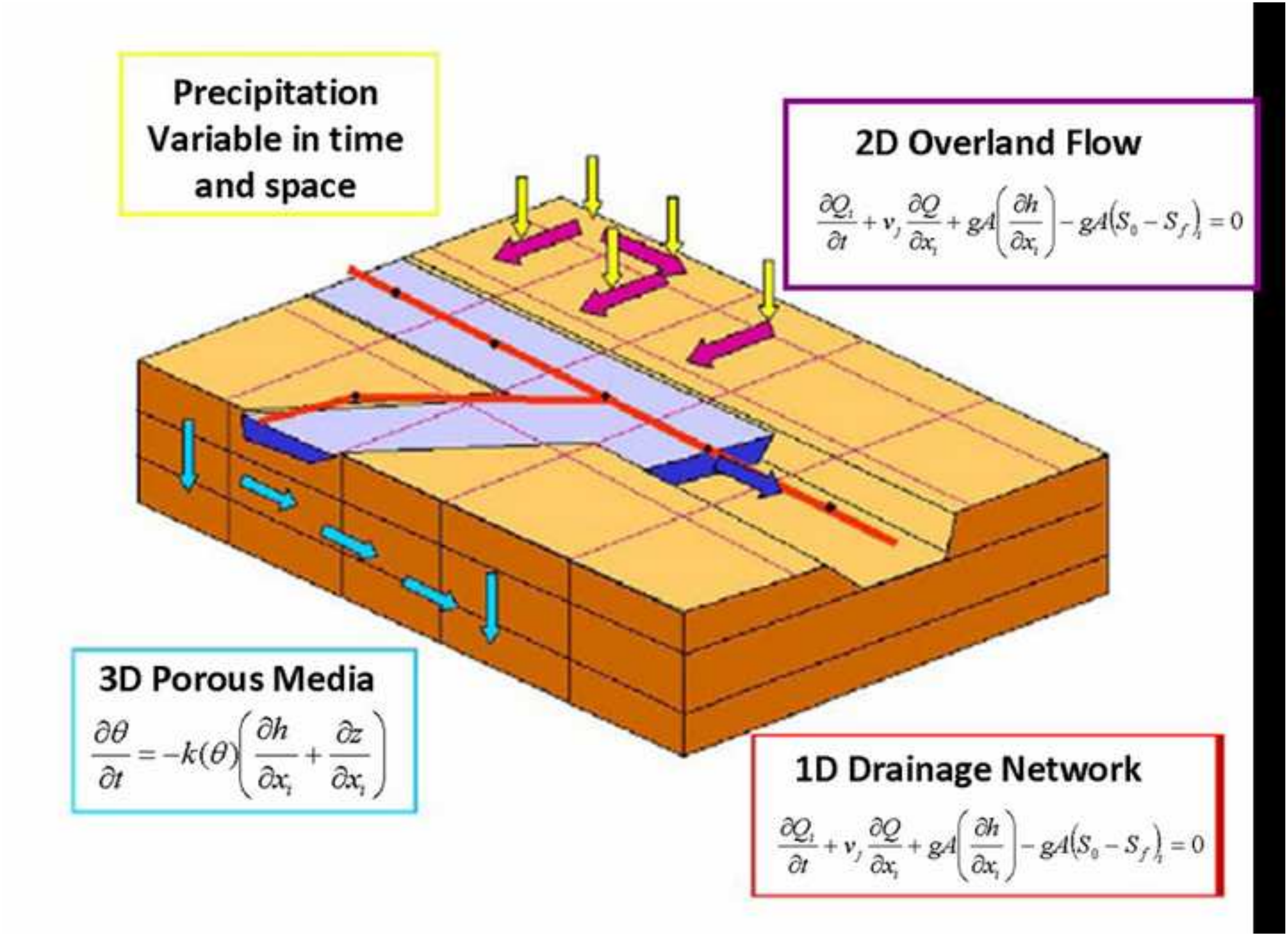

Figure10.TIF
Click here to download high resolution image

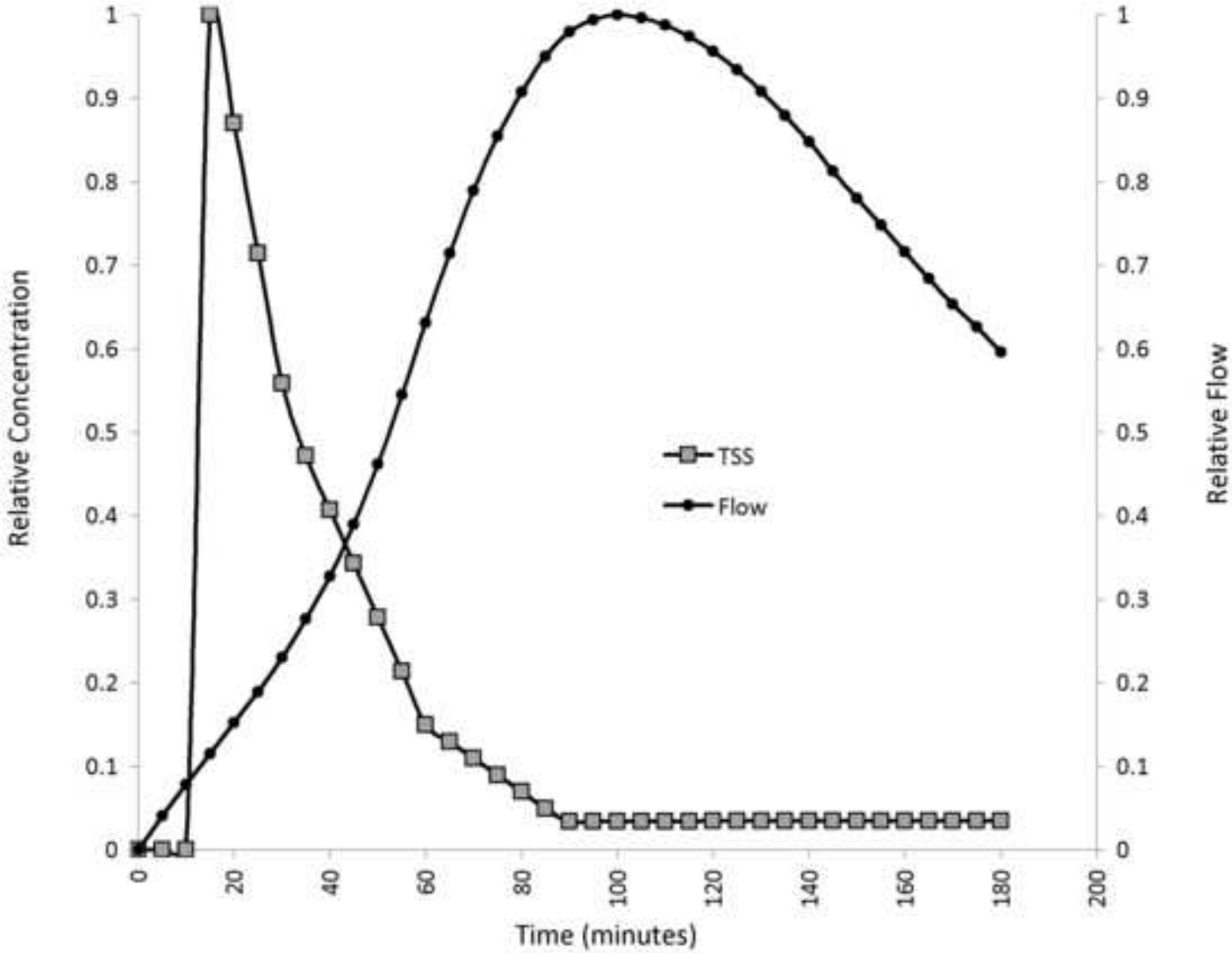

Figure2.tif
Click here to download high resolution image

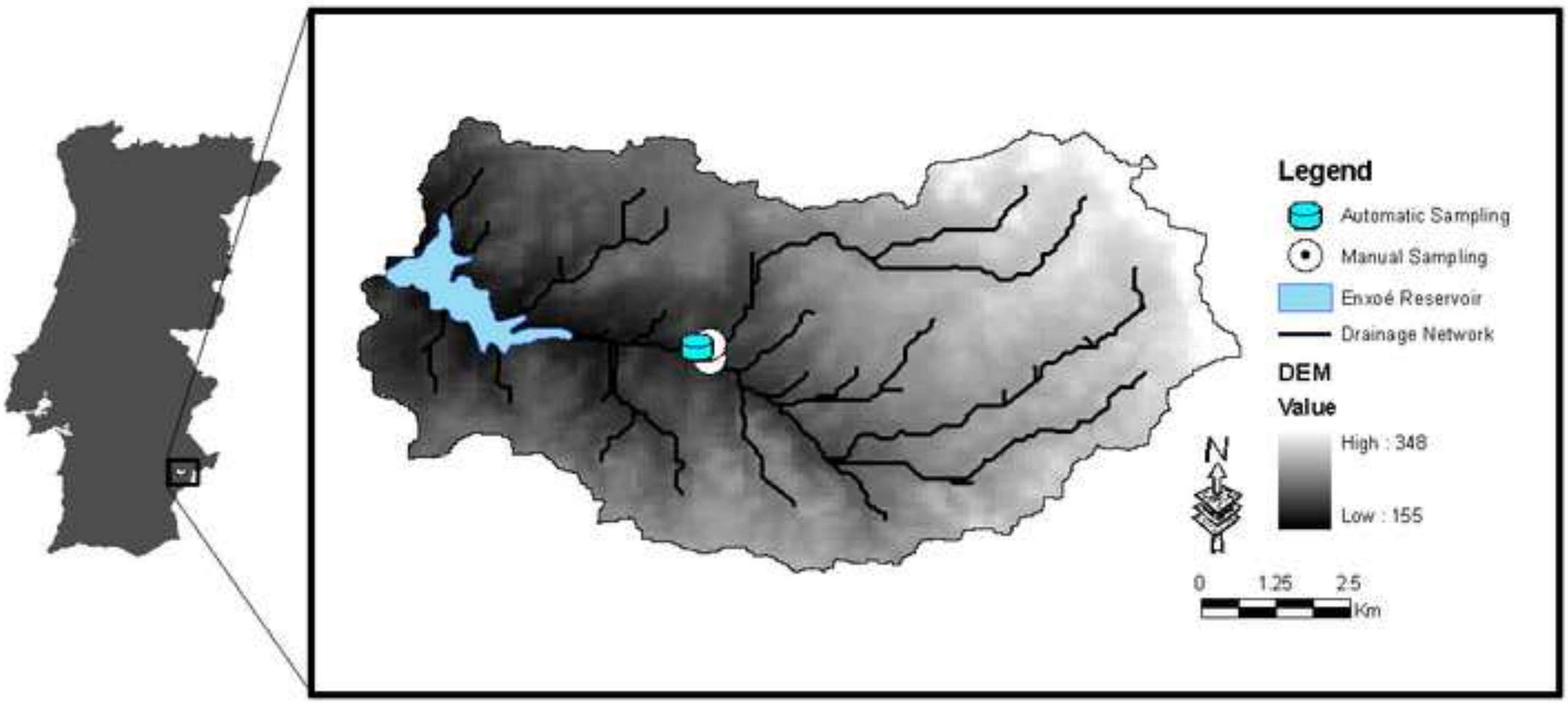

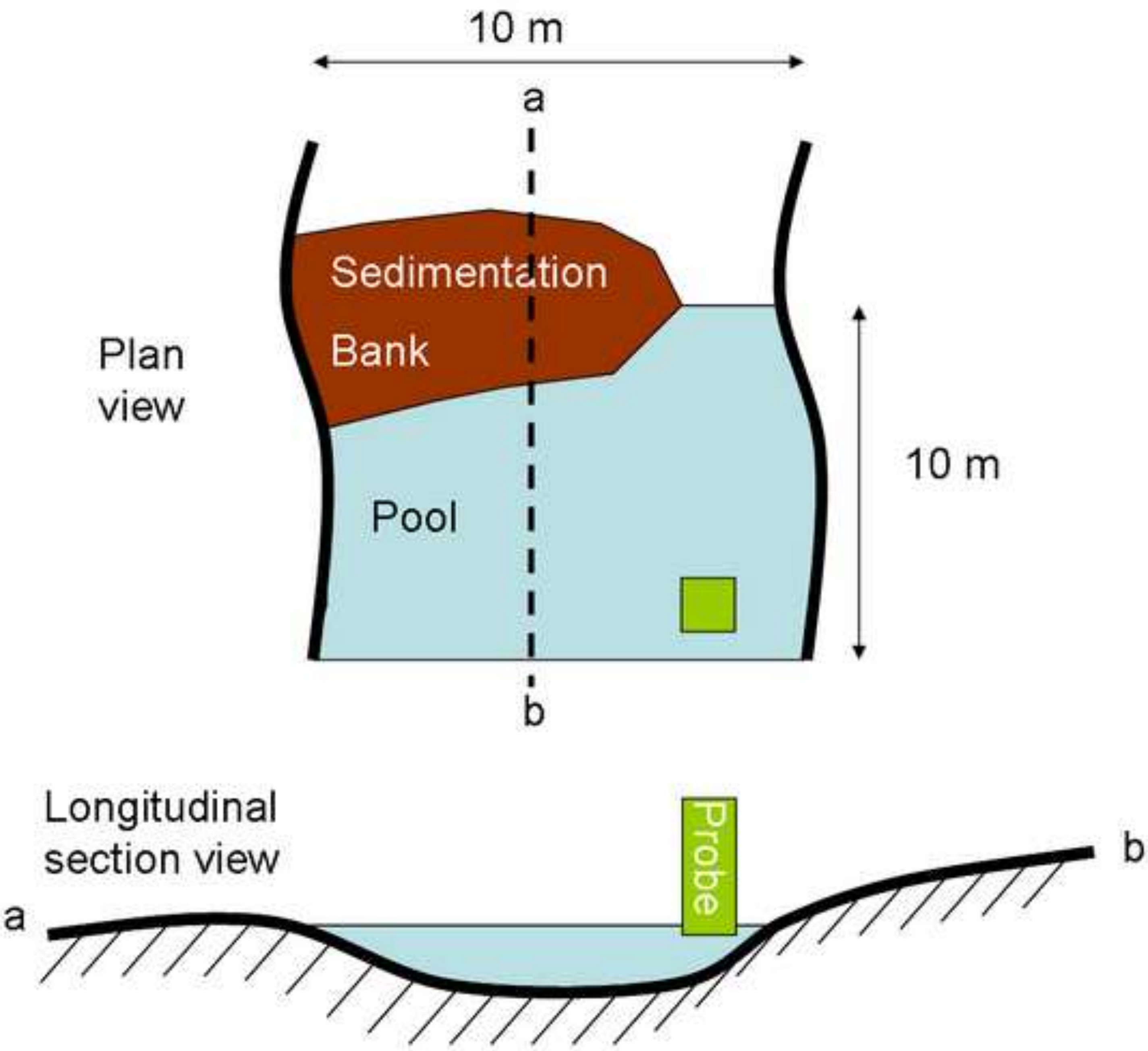
10 m
a
Sedimentation
Bank
Plan
view
Pool
10 m
b
Longitudinal
section view
Probe
a
b

Figure4.tif
Click here to download high resolution image

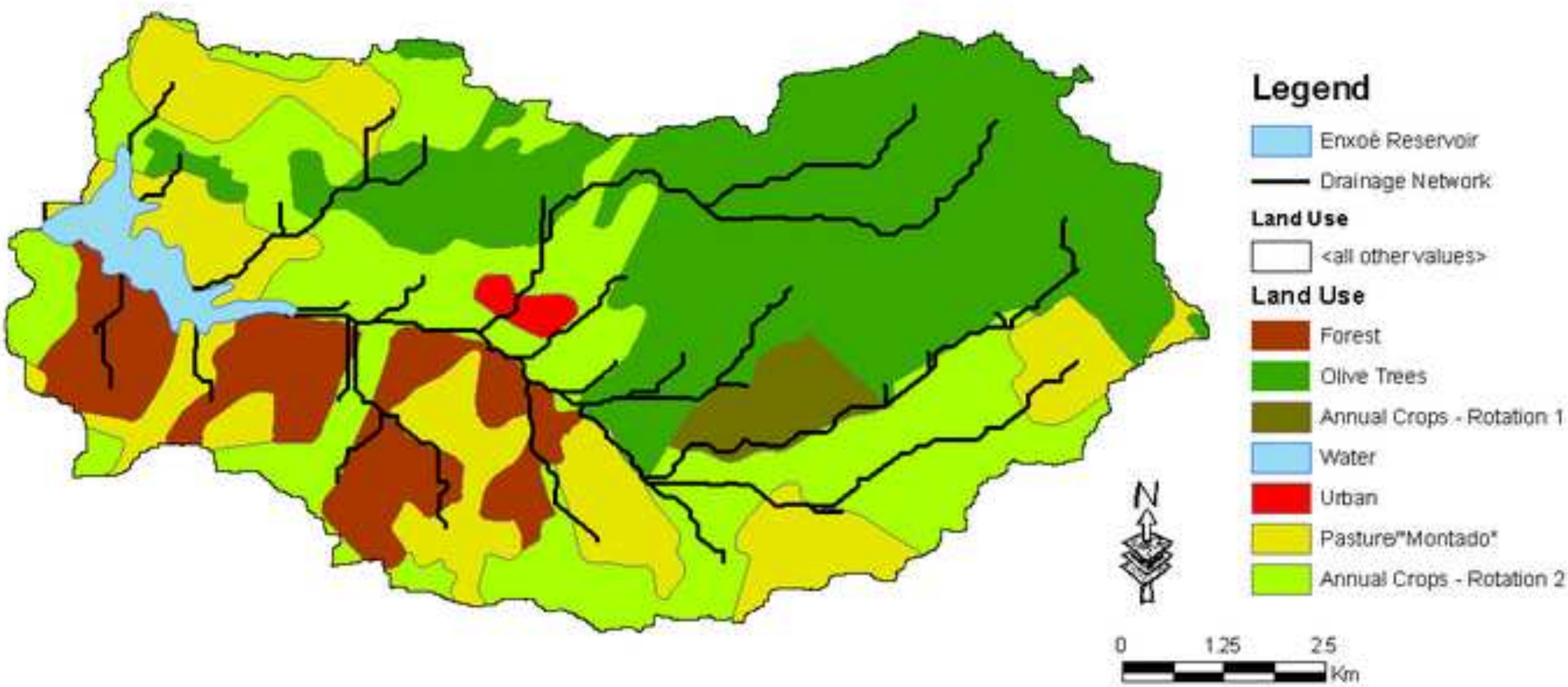

Figure4_B&W.tif

Click here to download high resolution image

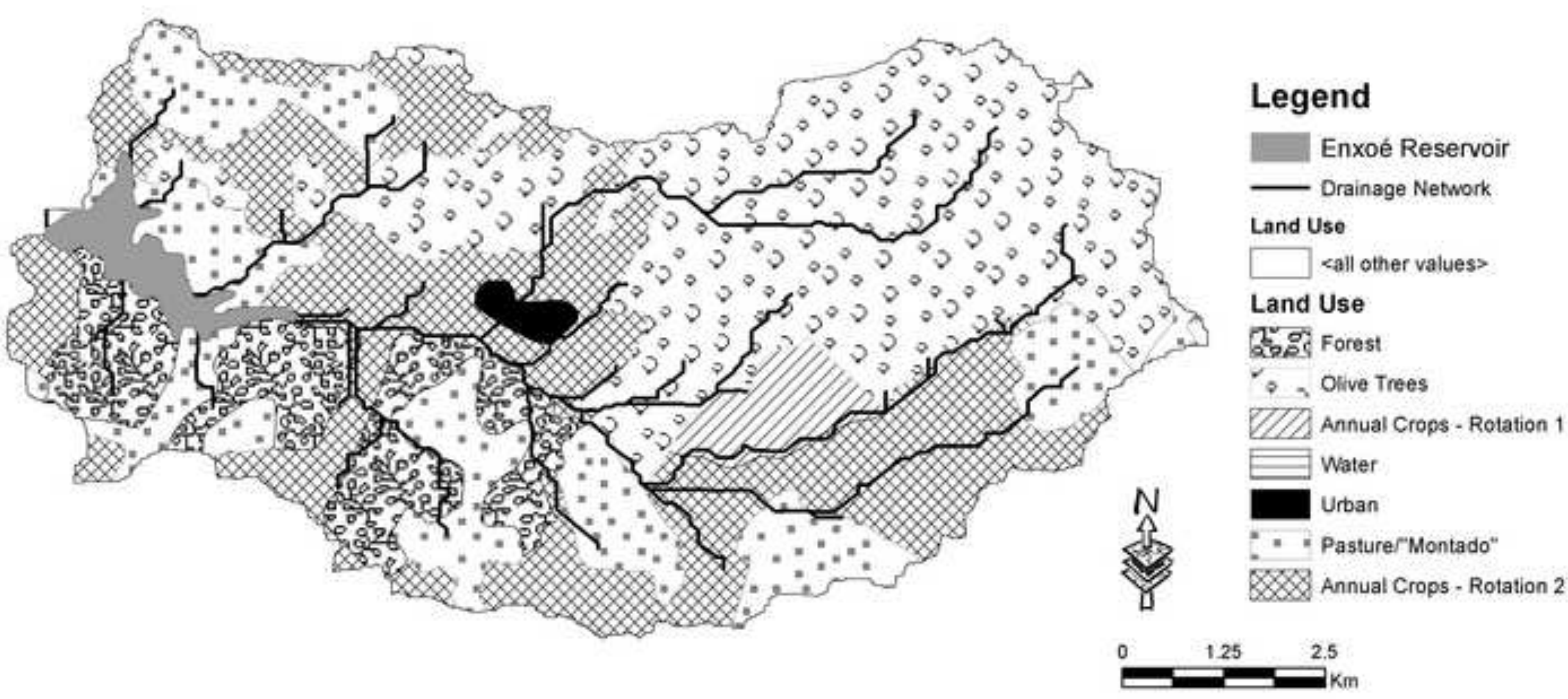

Figure5a.TIF

Click here to download high resolution image

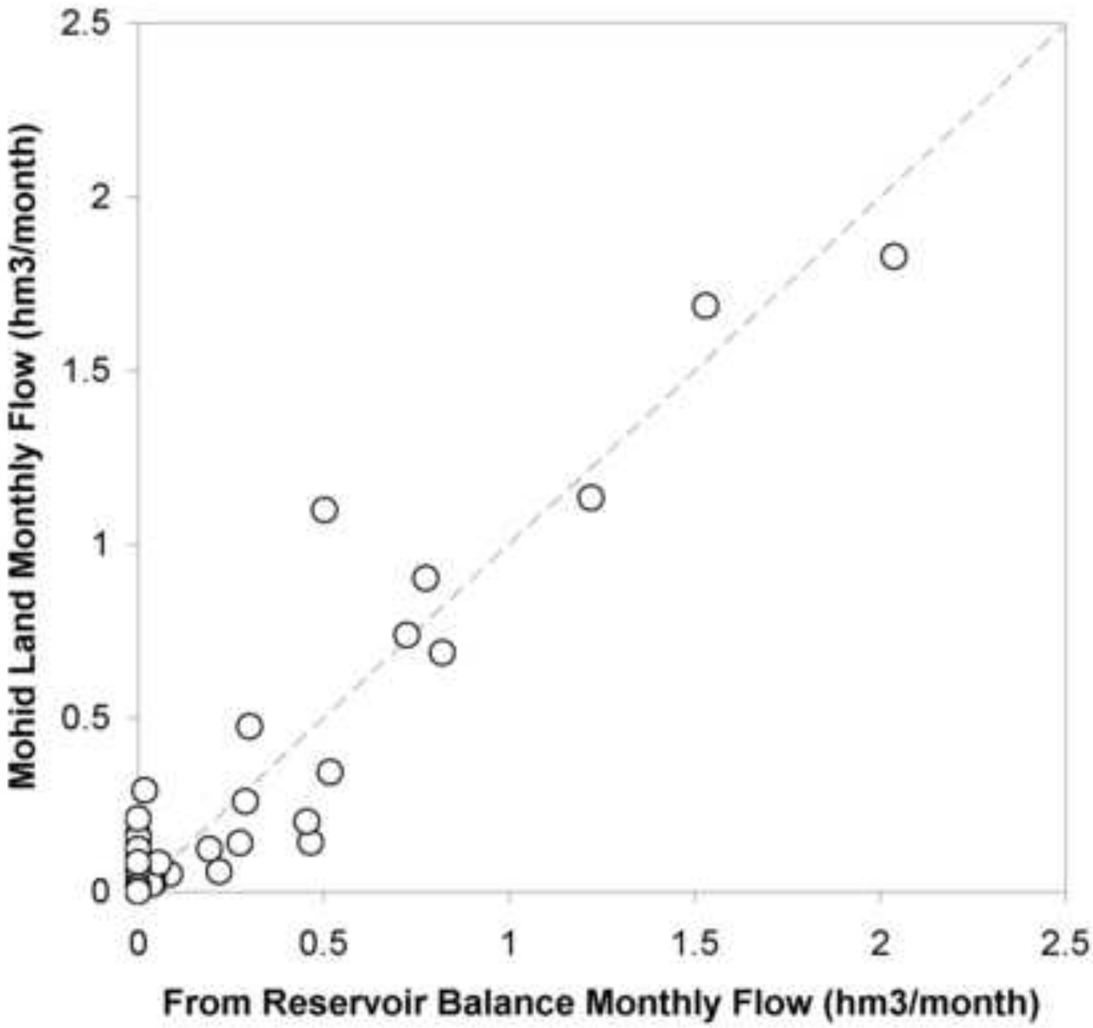

Figure5b.TIF
Click here to download high resolution image

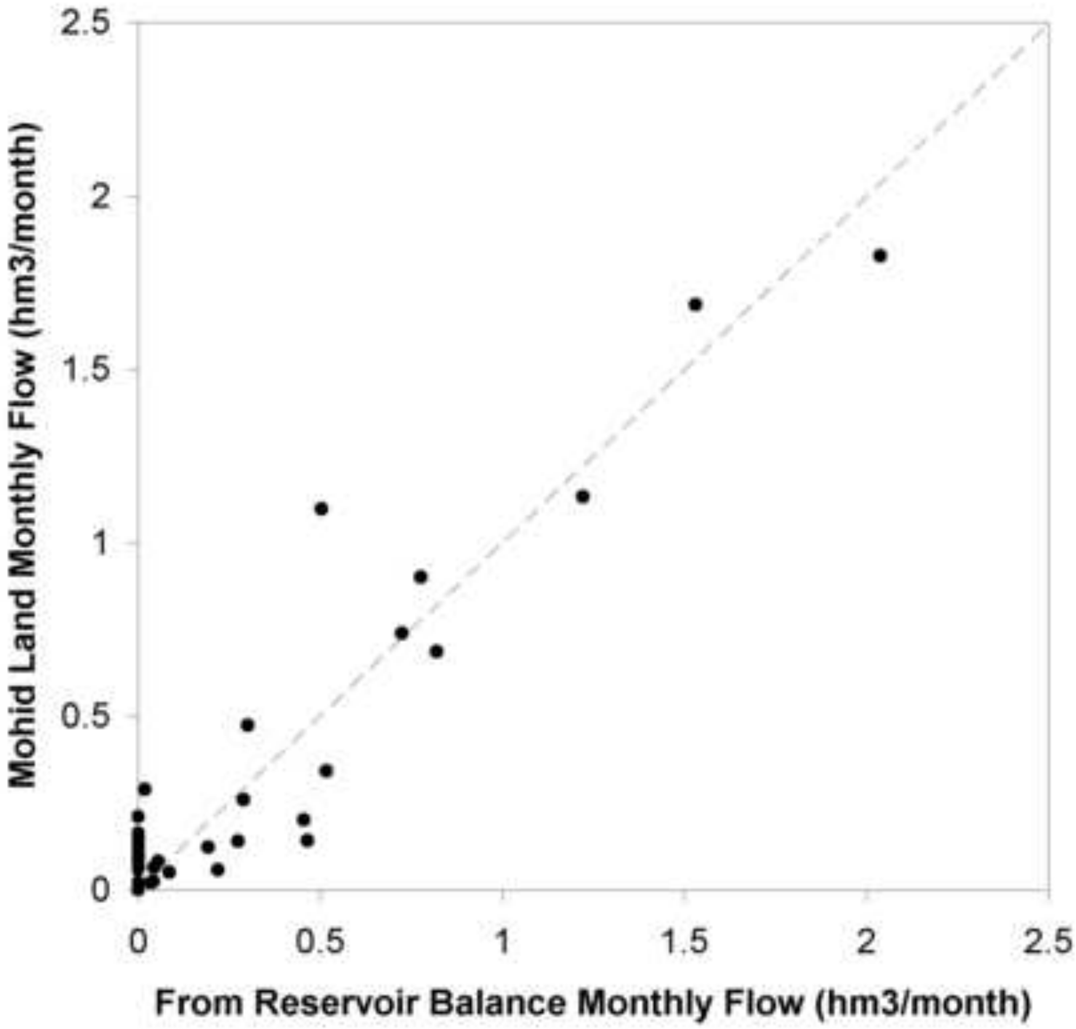

Figure6a.TIF

Click here to download high resolution image

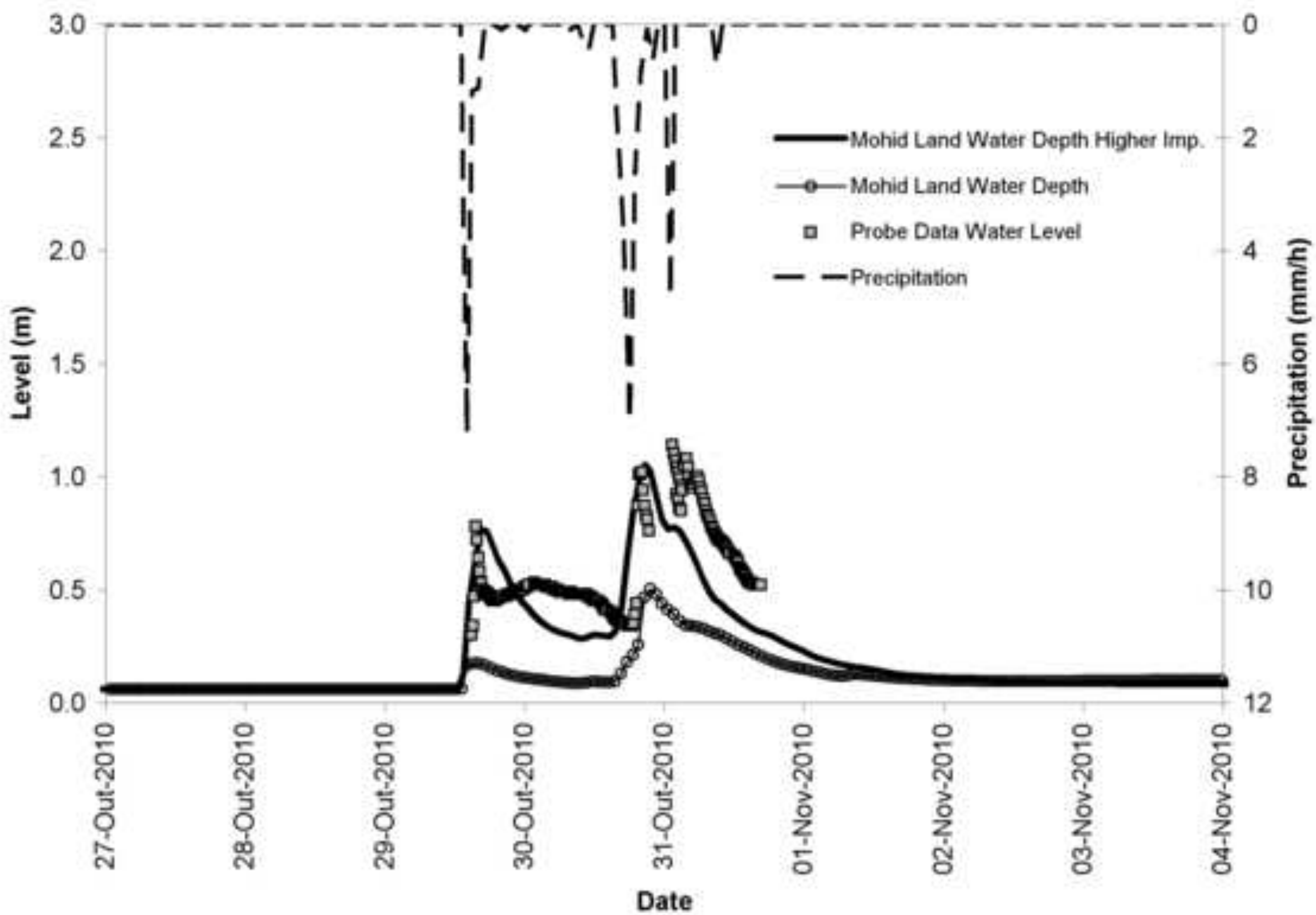

Figure6b.TIF
Click here to download high resolution image

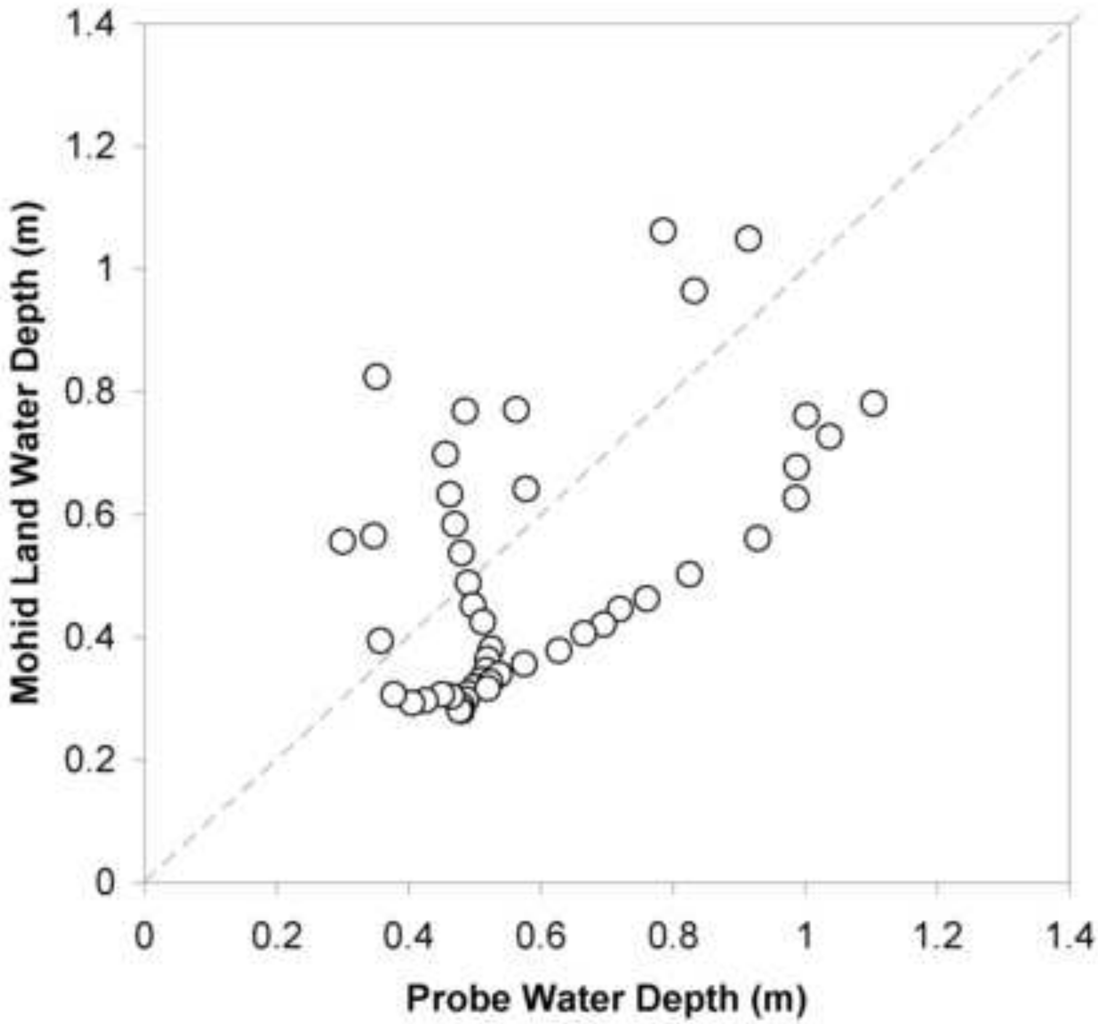

Figure7a.TIF
Click here to download high resolution image

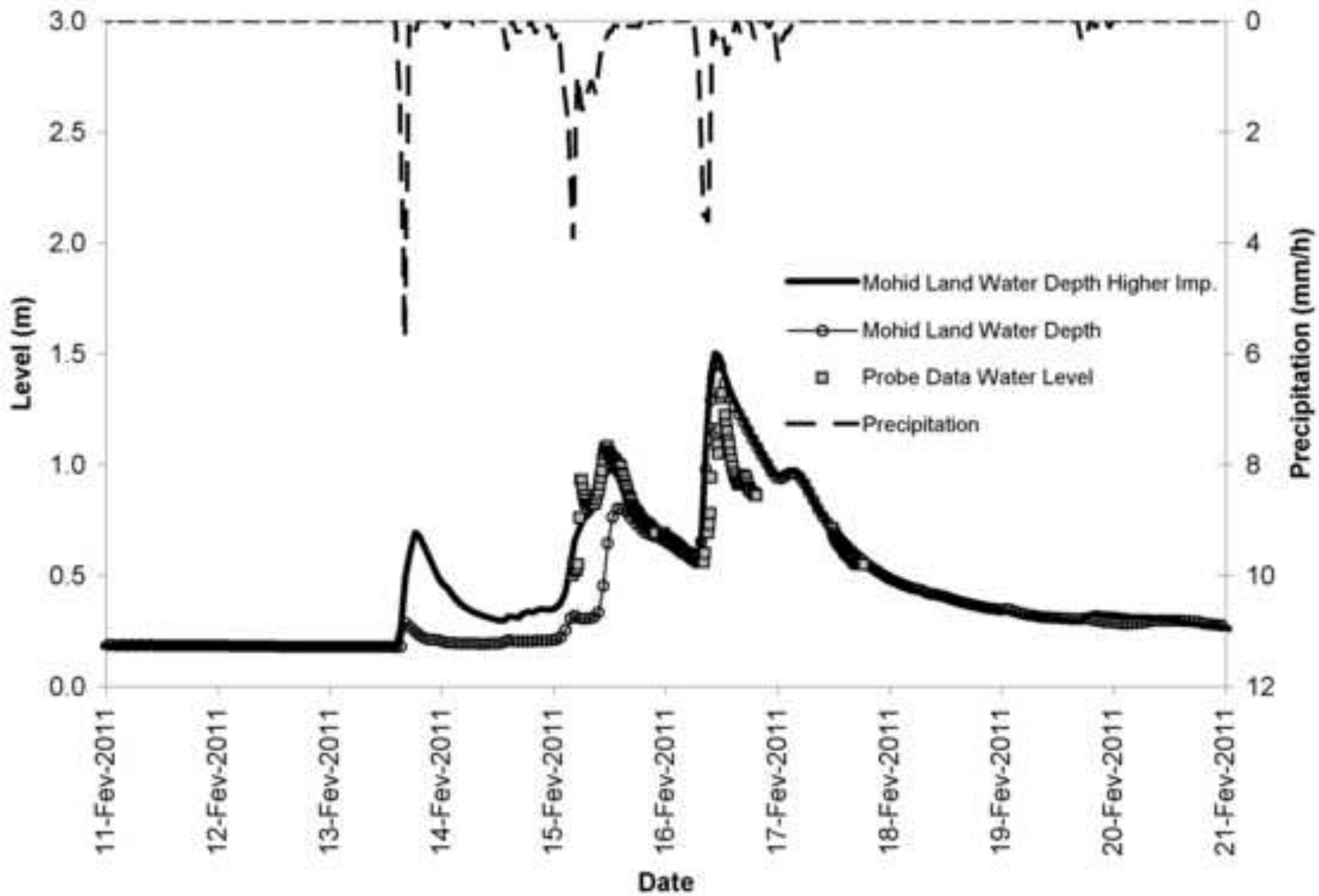

Figure7b.TIF
Click here to download high resolution image

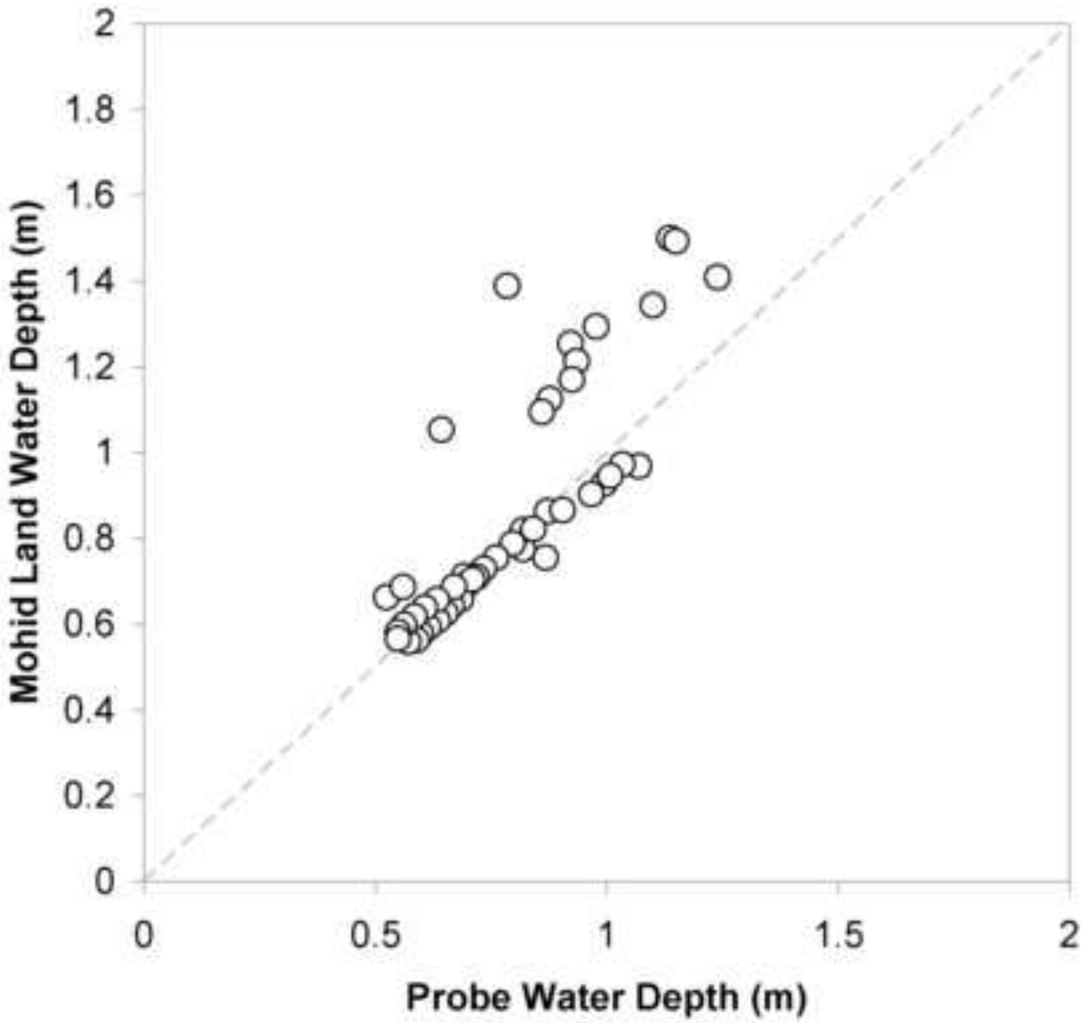

Figure8a.TIF

Click here to download high resolution image

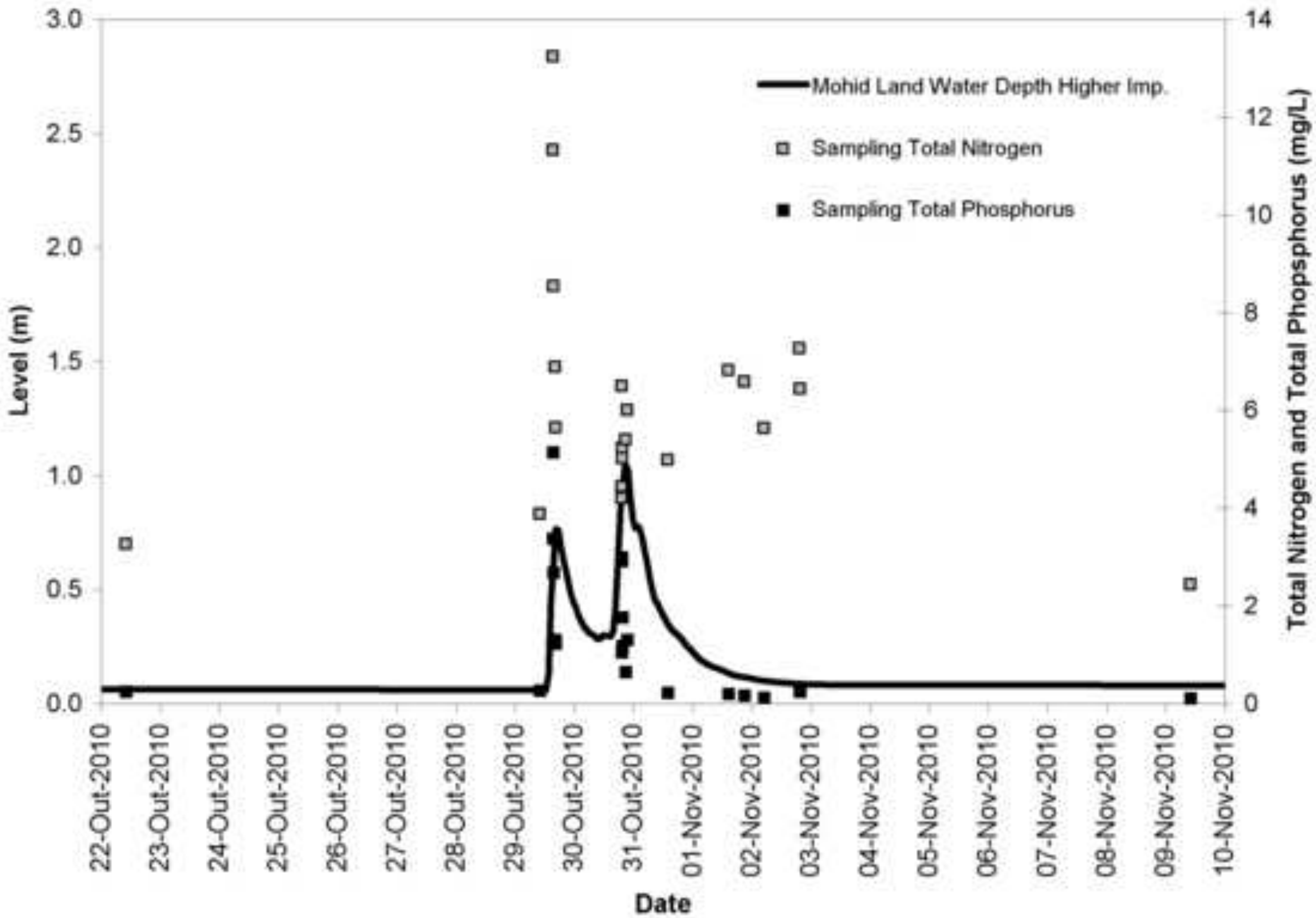

Figure8b.TIF
Click here to download high resolution image

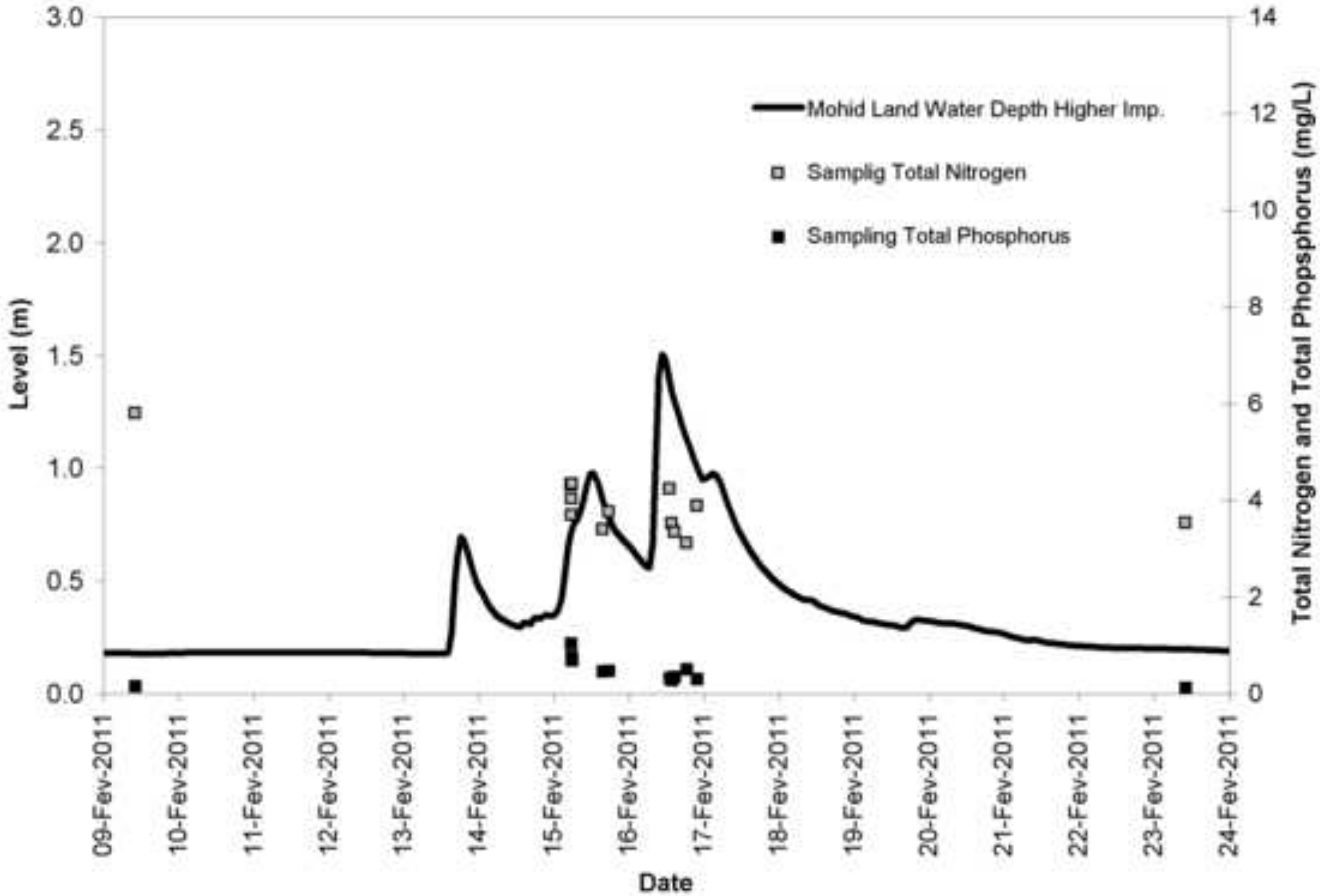

Figure9a.TIF
Click here to download high resolution image

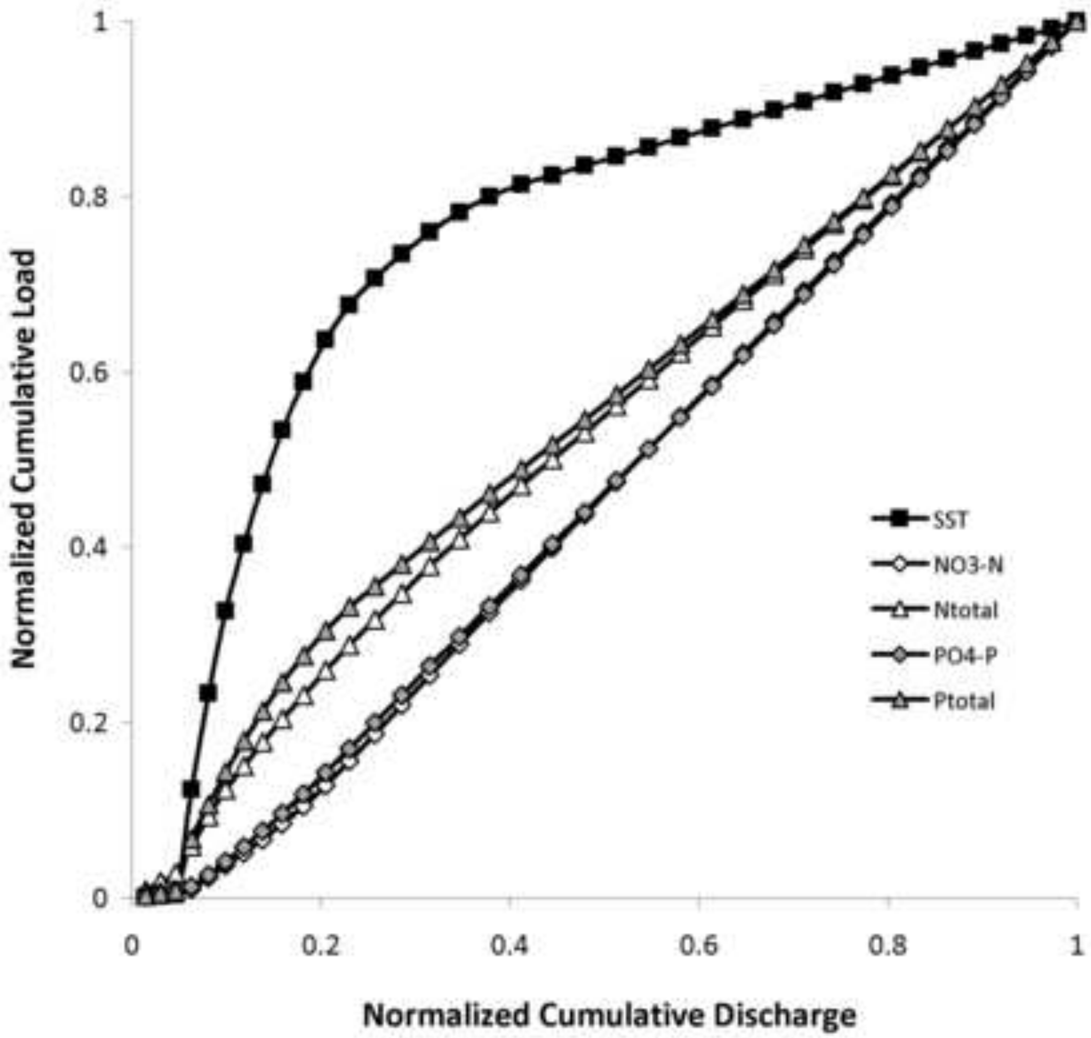

Figure9b.TIF

Click here to download high resolution image